TEAD1 is crucial for myelination, Remak bundles and functional regeneration of peripheral nerves

Matthew Grove[1], Hyukmin Kim[1], Shuhuan Pang[1], José Paz Amaya[2], Guoqing Hu[3], Jiliang Zhou[3], Michel Lemay[2], and Young-Jin Son[1]*

[1]Department of Neural Sciences, Shriners Hospitals Pediatric Research Center, Lewis Katz School of Medicine, Temple University, Philadelphia, PA 19140

[2]Department of Bioengineering, Temple University, Philadelphia, PA 19122, USA

[3]Department of Pharmacology & Toxicology, Medical College of Georgia, Augusta University, Augusta, GA

* Corresponding author: yson@temple.edu

ABSTRACT

The hippo pathway transcriptional effectors, YAP/TAZ, are crucial for Schwann cells (SCs) to myelinate axons but the mechanisms are poorly defined. Although TEAD1 has been implicated as a partner transcription factor, how it supports the transcriptional regulation of myelination and which aspects of the process it affects are unknown. Here, using conditional and inducible knockout mice, we report that TEAD1 is essential for SCs to develop, grow, and regenerate myelin sheaths. TEAD1/2/3/4 are present in SCs, but YAP/TAZ strongly favors TEAD1. It promotes myelination by positively and negatively regulating SC proliferation, enabling Krox20/Egr2 to upregulate myelin proteins, and upregulating the cholesterol biosynthetic enzymes FDPS and IDI1. We also show stage-dependent redundancy of TEAD1 and that non-myelinating SCs have a unique requirement for TEAD1 to enwrap nociceptive axons in Remak bundles. Our findings establish TEAD1 as a crucial partner of YAP/TAZ in developmental myelination and functional nerve regeneration and as a novel transcription factor regulating Remak bundle integrity.

ONE SENTENCE SUMMARY

TEAD1 in Schwann cells is a major transcriptional factor regulating peripheral nerve myelination and Remak bundle formation.

INTRODUCTION

In the mammalian peripheral nervous system, all motor and sensory axons are associated with Schwann cells (SCs). Axons larger than 1μm diameter are enveloped by myelinating SCs that form multilamellar myelin sheaths with a thickness proportional to axon caliber (*1, 2*). Axons smaller than 1μm diameter, the unmyelinated nociceptors (i.e., C-fibers), are organized in clusters called Remak bundles, in which each C-fiber is ensheathed by a cytoplasmic pocket formed by non-myelinating SCs, also known as Remak SCs (*3, 4*). Both myelinating and non-myelinating SCs provide metabolic and functional support essential for structural and functional integrity of peripheral nerves. Failure to initiate or maintain proper axon-SC association may lead to life-threatening paralysis and peripheral neuropathy (*5*). Myelinating SCs form and

54 maintain myelin via a set of key transcription factors (TFs) and regulators (*6-12*). However, the
55 transcriptional regulation of myelinating SCs remains incompletely understood, and that of non-
56 myelinating SCs is largely unknown (*4*).

57 Recent mouse genetic studies surprisingly revealed that YAP (Yes-associated protein)
58 and its paralogue, TAZ (Transcriptional coactivator with PDZ-binding motif), which are potent
59 oncoproteins and transcriptional regulators in the Hippo signaling pathway, play crucial roles in
60 developing, maintaining, and regenerating myelination of peripheral nerves. Both YAP and TAZ
61 (YAP/TAZ) are expressed initially in all immature SCs and then selectively in myelinating SCs
62 (*13*). The processes for which they are required include: timely sorting of large axons and
63 associated SC proliferation (*13, 14*); initiation of SC differentiation or myelination (*13, 15*);
64 myelin maintenance in adults (*13*); and remyelination following nerve injury (*16, 17*). YAP/TAZ
65 initiate and maintain myelination in part by upregulating Krox20 (a.k.a., Egr2) (*13, 18*), which is
66 widely recognized as the master TF promoting peripheral myelination. Krox20 is required to
67 initiate myelination, maintain adult myelin (*7, 19*), and likely to promote myelin sheath growth
68 (*20*). It acts through direct transcriptional upregulation of myelin proteins and membrane lipids
69 (*21-23*).

70 YAP/TAZ are transcriptional co-activators that contain a transcriptional activation
71 domain, but no DNA binding domain. They regulate gene expression by binding to partner TFs,
72 typically members of the TEA domain family (TEAD1-4) (*24*). Conversely, TEADs on their
73 own are unable to activate or repress transcription (*25*) and require the help of co-factors such as
74 YAP/TAZ to act (*26*). Partner TFs such as TEADs are required to maintain YAP/TAZ in the
75 nucleus, which keeps them transcriptionally active (*27-30*). Transcript data indicates that SCs
76 express all four TEADs and that their expression peaks at different times during development
77 (*31*). Moreover, TEAD1-4 show unique, redundant, and/or opposing roles in regulating
78 proliferation and differentiation of various cell types; these roles can also change as a function of
79 developmental stage (*26, 32-34*). It remains to be elucidated how and which TEAD(s) in SCs
80 mediate transcriptional regulation of YAP/TAZ for the development, homeostasis, and/or
81 regeneration of myelination.

82 In some cells, TEAD1 serves as the main partner TEAD and plays non-redundant roles
83 (*35, 36*). In SCs, ChiP, co-IP, and transcription assays have consistently indicated that TEAD1
84 associates with YAP/TAZ for upregulating myelin proteins (*13, 18, 37, 38*). Notably, unlike

85 YAP/TAZ, TEAD1 is expressed in all SC nuclei (*13*), suggesting that, independently of
86 YAP/TAZ, TEAD1 plays an unknown role in non-myelinating SCs. In this study, we generated
87 conditional and inducible knockout mice lacking TEAD1 in SCs to investigate the roles of
88 TEAD1 in myelinating and non-myelinating SCs. We found that TEAD1 is uniquely required for
89 myelinating SCs to initiate, grow and regenerate myelination, and for non-myelinating SCs to
90 enwrap C-fibers in Remak bundles during development and homeostasis. We also uncovered the
91 mechanistic basis of the non-redundancy of TEAD1 and found that YAP/TAZ-TEAD1 promotes
92 myelination by dually regulating SC proliferation, by enabling induced Krox20 to upregulate
93 myelin proteins and by upregulating cholesterol biosynthetic enzymes. Additional results suggest
94 that other TEADs may play redundant and opposing roles in a stage-dependent manner.
95
96 **RESULTS**
97
98 **Multiple TEADs are expressed in Schwann cells of WT, *Tead1* cKO and iKO mice**
99 To investigate the roles of SC TEAD1 in developing nerves, we conditionally ablated
100 *Tead1* by crossing *Tead1*$^{fl/fl}$ mice (*39*) with mice carrying *Mpz*-Cre, which is active from E13.5 in
101 SCs (*40*). To investigate the roles of TEAD1 in maintaining and regenerating nerves in adults,
102 we inducibly inactivated SC *Tead1* by crossing *Tead1*$^{fl/fl}$ mice with mice carrying a tamoxifen-
103 inducible *Plp*-CreER (*41*). Immunostaining of P22 WT and *Mpz-Cre;Tead1*$^{fl/fl}$ (hereafter *Tead1*
104 cKO) sciatic nerves (SNs) showed that TEAD1 was expressed in the nuclei of 100% of WT SCs
105 and was undetectable in >97% *Tead1* cKO SCs (Figure 1A). Immunostaining of WT and *Plp* -
106 CreER*; Tead1*$^{fl/fl}$ (hereafter *Tead1* iKO) SNs after tamoxifen treatment showed that TEAD1 was
107 also present in 100% of SC nuclei in both intact and regenerating nerves of adult WT mice and
108 was deleted in almost all *Tead1* iKO SCs (Figure 1B, 1C). The specificity of the TEAD1
109 immunostaining and highly efficient deletion were further confirmed by Western blotting (Figure
110 1D). These results suggest potential roles for TEAD1 in both myelinating and non-myelinating
111 SCs during development, maintenance and after nerve injury.
112 To investigate the expression of other TEADs in WT, *Tead1* cKO and *Tead1* iKO SCs,
113 we used antibodies to TEAD2, 3 and 4, and a pan-TEAD antibody marketed to recognize all four
114 TEADs (TEAD1/2/3/4). Western blot analysis of SN lysates showed that anti-TEAD3 and anti-
115 pan TEAD both revealed a main ~ 50kD band that was decreased in *Tead1* cKO (Figure 1D).

116 The pan-TEAD antibody may therefore bind preferentially to TEAD3. Anti-TEAD4 recognized
117 three bands in WT and showed that the two faster-migrating bands were decreased in *Tead1* cKO
118 (Figure 1D). Anti-TEAD2 recognized a band of ~65 kD in *Tead1* cKO that was barely detectable
119 in WT lysates. This band corresponded to the size of TEAD2 reported in other cell types (*42*).
120 We also found that the ~65 kD band was present early postnatally, but rapidly diminished with
121 age (data not shown), consistent with previous transcript data from mouse SCs (*31*). Therefore,
122 the expression of TEAD2-4 was altered in *Tead1* cKO, confirming the specificity of the
123 antibodies and their expression in SCs. Of these anti-TEAD antibodies, only anti-pan TEAD
124 functioned effectively for immunofluorescence staining, verifying the presence of other TEADs
125 in SC nuclei in both intact (Figure 1E) and injured WT and *Tead1* iKO SNs (Figure 1F). These
126 results suggest that WT SCs express all four TEADs and that *Tead1* cKO and iKO SCs express
127 TEAD2-4 in their nuclei.
128
129 **YAP/TAZ strongly favor TEAD1 but partner with other TEADs in the absence of TEAD1**
130 In the absence of a partner TF, nuclear YAP/TAZ are decreased and phosphorylation of
131 YAP/TAZ increased, due to targeting by Large tumor suppressor kinase 1/2 (LATS1/2),
132 negative regulators of YAP/TAZ (*43*). To investigate if YAP/TAZ are in the nuclei of SCs and
133 therefore transcriptionally functional in the absence of TEAD1, we compared western blotting of
134 P50 WT vs *Tead1* cKO SN lysates and observed an overall decrease in YAP levels in *Tead1*
135 cKO but a > 2-fold increase in TAZ levels compared to WT (Figure 2A). This ratio of YAP to
136 TAZ in *Tead1* cKO resembled that observed during developmental myelination in WT SNs (*13,*
137 *15*). Furthermore, phosphorylation of YAP decreased in cKO, which would typically indicate
138 increased YAP activity. These results suggest that YAP/TAZ are not targeted for destruction in
139 the absence of TEAD1. Indeed, YAP/TAZ were retained in the SC nucleus of *Tead1* cKO
140 (Figure 2B) and both intact and injured *Tead1* iKO SNs (Figure 2C, 2D), as strongly supported
141 by quantitative analysis (Figure 2E).
142 To investigate whether other TEADs could be complexed with YAP/TAZ, thereby
143 retaining YAP/TAZ in SC nuclei in the absence of TEAD1, we carried out YAP/TAZ co-
144 immunoprecipitation (IP) experiments comparing WT vs *Tead1* iKO, and blotted for YAP/TAZ,
145 TEAD1 and pan-TEAD (Figure 2F). After verifying equal amounts of lysate samples and the
146 efficiency of IPs with post-IP lysates, we observed that TEAD1 strongly co-IPed with YAP/TAZ

147 from WT lysates and that levels were greatly reduced in *Tead1* iKO lysates. Blotting with anti-
148 pan-TEAD showed that multiple TEADs were co-IPed with YAP/TAZ from both WT and *Tead1*
149 iKO lysates. Notably, the pan-TEAD co-IPed from WT lysates, like TEAD1, migrated more
150 slowly than that from *Tead1* iKO lysates, whereas the *Tead1* iKO pan-TEAD migrated similarly
151 to the major pan-TEAD band in post-IP lysates. Longer exposure of the pan-TEAD film revealed
152 the presence of a fainter band migrating above the main pan-TEAD band in WT lysates (Figure
153 2F; arrow). Because this band co-migrated with TEAD1 and was not present in *Tead1* iKO
154 lysates, it was identified as TEAD1. These results suggest that TEAD1 makes up a very minor
155 portion of that revealed by pan-TEAD in WT lysates, but the overwhelming majority of that
156 revealed by pan-TEAD in YAP/TAZ IPs from these lysates. Therefore, although multiple
157 TEADs are present, TEAD1 is greatly favored as the binding partner for YAP/TAZ. However, in
158 the absence of TEAD1, other TEADs are associated with YAP/TAZ presumably to substitute for
159 some or all the functions of the YAP/TAZ-TEAD1 transcriptional complex.
160
161 **TEAD1 is required for myelin sheath formation and growth**
162 *Tead1* cKO mice were smaller than WT mice at all ages, with labored breathing and
163 severely splayed fore- and hindlimbs, indicative of severe peripheral neuropathy (Figure 3A,
164 Supplementary Video 1). The hindlimbs never became completely paralyzed, however, in
165 contrast to *Yap/Taz* cDKO mice (*13*). *Tead1* cKO mice were humanely euthanized before P60.
166 *Tead1* cKO SNs were noticeably translucent, indicative of reduced myelin content (Figure 3B).
167 Electrical stimulation of cKO SNs elicited low and dispersed compound muscle action potentials
168 (CMAPs) (Figure 3C). Nerve conduction velocity (NCV) in cKO was ~8 m/s, which was
169 markedly reduced from ~40 m/s in WT mice (Figure 3D).
170 Next, we used semi-thin and transmission electron microscopy (TEM) to examine the
171 processes of developmental myelination and Remak bundle formation. We first examined SNs at
172 P3, when, in WT, many large axons had already been radially sorted, establishing 1:1
173 relationship with promyelinating SCs, and myelination had begun. Compared to WT, *Tead1* cKO
174 SNs were thinner, unsorted bundles of axons were larger and more numerous, and myelination
175 was minimal (Figure 3E). Nevertheless, we frequently observed large axons that had been sorted
176 and established a 1:1 relationship with promyelinating SCs, as in WT. Therefore, radial sorting

177 was delayed in *Tead1* cKO, though less severely than in *Yap/Taz* cDKO mice, in which no axons
178 were sorted at P4 (*13*).
179 At P22, when WT SNs were fully myelinated, the phenotype of *Tead1* cKO SNs was
180 complex and included areas of unsorted axon bundles, sorted but unmyelinated axons, and thinly
181 myelinated axons (Figure 3F, Supplementary figure 1A). Notably, at P50, this phenotype was
182 unchanged from that at P22: areas of unsorted bundles, promyelination, and thin myelination
183 persisted (Figure 3G, Supplementary figure 1A). TEM analysis confirmed that myelin was
184 indeed thinner in *Tead1* cKO than in WT at both P22 and P50 (Figure 3F, 3G, Supplementary
185 figure 1B). The g-ratio did not significantly change in either WT or cKO between P22 and P50
186 (Figure 3H), suggesting that growth of the myelin sheath relative to axon diameter did not
187 increase over this period. These data suggest that myelination in *Tead1* cKO was arrested rather
188 than delayed. Plots of g-ratio versus axon diameter showed that the mutant defect was present in
189 axons of all diameters but was particularly notable in those of larger diameter (Figure 3I, 3J).
190 The mean axon diameter was also reduced in cKO at P22, though it increased with age (Figure
191 3K). These data show that TEAD1 is required, like YAP/TAZ (*13*), for timely radial sorting and
192 initiation of myelination during development. Although some axons become myelinated in the
193 absence of TEAD1, presumably due to other TEADs, they require TEAD1 for myelin sheath to
194 properly grow in proportion to axon diameter.
195
196 **TEAD1 is required for proper formation of Remak bundles**
197 Remak bundle formation was also abnormal in *Tead1* cKO mice. In WT SNs at P22 and
198 P50, small diameter axons were present in Remak bundles, with each C-fiber ensheathed by SC
199 cytoplasm (Figure 3F, 3L). In *Tead1* cKO, C-fibers were also present in bundles in which axons
200 were rarely larger than 1 μm in diameter, suggesting that they were almost fully sorted.
201 However, at both P22 and P50, the observed bundles were frequently small, often the size of a
202 large myelinated axon. Notably, a SC surrounded each bundle but individual C-fibers of most
203 Remak bundles were not ensheathed by SC cytoplasm (Figure 3L). Furthermore, these bundles
204 were frequently and abnormally thinly myelinated. Quantification showed that ~80% of C-fibers
205 were not ensheathed by SC cytoplasm in P50 *Tead1* cKO SNs (Figure 3M). Therefore, TEAD1
206 is required to develop proper association of C-fibers with non-myelinating SCs in Remak
207 bundles.

208

209 **TEAD1 regulates SC proliferation both positively and negatively to promote myelination**

210 For myelination and Remak bundle formation to occur properly, timely generation of
211 sufficient numbers of SCs is essential. YAP/TAZ are necessary for optimal SC proliferation in
212 the late embryonic and early postnatal periods (*13, 15, 44*). To determine if the defects of
213 myelination and Remak bundles in *Tead1* cKO are due to defective SC proliferation, we counted
214 SCs. At P3, SC number in cKO SNs was about half that of WT (Figure 4A), slightly more than
215 in *Yap/Taz* cDKO at P4 (*13*). The number of SCs in the cell cycle (Ki67-positive; Figure 4B) and
216 in S-phase (EdU-positive; Figure 4C) was greatly reduced in cKO at P3. Therefore, TEAD1 is
217 required for optimal SC proliferation at P3, suggesting that the YAP/TAZ-TEAD1 complex
218 promotes SC proliferation at early postnatal periods.

219 At P22 and P50, however, SC numbers in *Tead1* cKO SNs were greatly increased and
220 became more than twice those of WT (Figure 4A); a similar increase was not observed in
221 *Yap/Taz* cDKO (*13*). As *Tead1* cKO SC numbers were similar at P22 and P50, we reasoned that
222 between P3 and P22, SC proliferation must occur at an abnormally high rate in this mutant.
223 Indeed, the number of SCs that were Ki67-positive or EdU-positive was significantly increased
224 in cKO at P22 (Figure 4B, 4C). The increased SC numbers were not due to proliferation of
225 residual non-deleted SCs: whereas in WT, EdU-positive SCs contained TEAD1, TEAD1 was
226 absent in most EdU-positive SCs in *Tead1* cKO (Figure 4D). During development, therefore,
227 SCs switch from requiring TEAD1 for optimal proliferation, to requiring TEAD1 for timely exit
228 from the cell-cycle, which is a prerequisite for SC differentiation and myelination (*45*).

229

230 **TEAD1 is required for Krox20 to upregulate myelin proteins, but not for Krox20**
231 **upregulation**

232 Our findings thus far show that, in the absence of TEAD1 in SCs, other TEADs can
233 complex with YAP/TAZ. Nevertheless, only some axons are myelinated abnormally thinly in
234 *Tead1* cKO which grossly phenocopied *Yap/Taz* iDKO. These defects are not because *Tead1*
235 cKO mice lack SCs. *Yap/Taz* cDKO exhibited a complete failure of myelination due to arrest of
236 their SCs as promyelinating SCs, in part because they fail to upregulate Krox20/Egr2 (Early
237 Growth Response 2), which drives transcription of myelin proteins (*13*). To determine whether
238 TEAD1 is required for Krox20 upregulation, we first investigated Oct6 (Pou3f1, Scip), whose

239 upregulation precedes and is required for Krox20 upregulation; Oct6 is subsequently
240 downregulated, possibly by Krox20 in a feedback mechanism (*46, 47*). Western blotting of P50
241 SN lysates showed minimal expression of Oct6 in WT, but greatly upregulated expression in
242 *Tead1* cKO (Figure 5A). Immunohistochemistry of P50 cKO SNs showed intense Oct6
243 expression in ~80% of SC nuclei; Oct6 expression was minimal in WT (Figure 5B). Notably, at
244 both P11 and P50, a similar percentage of SCs expressed Krox20 in WT and *Tead1* cKO SNs
245 (Figure 5C). In Western blots, Krox20 was upregulated >4-fold in cKO compared to WT (Figure
246 5A). As adult *Tead1* cKO mice contain ~2-fold more SCs than WT (Figure 4A), these data
247 suggest that each SC in *Tead1* cKO contains ~2-fold more Krox20 than WT. Thus, in contrast to
248 SCs lacking YAP/TAZ (*13*), SCs lacking TEAD1 upregulate Krox20, suggesting that TEAD1 is
249 dispensable for YAP/TAZ to upregulate Krox20.
250 Consistent with the idea that Krox20 is pivotal for myelin gene transcription, expression
251 of myelin basic protein, MBP, and myelin protein zero, MPZ, was abundant in WT P50 SNs
252 (Figure 5A). In contrast, despite ample expression of Krox20, both MBP and MPZ were
253 markedly decreased in *Tead1* cKO, suggesting that Krox20 fails to properly upregulate myelin
254 proteins without TEAD1. To exclude the possibility that Krox20 expressed in cKO SCs is
255 defective, we took advantage of the earlier finding that loss of Krox20 or its co-factors, Nab1/2,
256 causes SCs to remain aberrantly in the cell-cycle (*12, 47*). Therefore, we studied whether EdU-
257 positive SCs in the cell-cycle of P11 cKO were also positive for Krox20, which would indicate
258 defective Krox20. We found that, although ~65% of SC nuclei contained Krox20, only a few
259 EdU-positive SCs exhibited even minimal Krox20 immunoreactivity in either WT or *Tead1* cKO
260 (Figure 5D). Thus, despite high levels of functional Krox20, myelin protein expression was
261 greatly reduced in cKO SCs, suggesting that TEAD1 is dispensable for Krox20 upregulation but
262 required for Krox20 to upregulate myelin proteins.
263
264 **TEAD1 and YAP/TAZ upregulate cholesterol biosynthetic enzymes, FDPS and IDI1**
265 Myelination of peripheral nerves by SCs requires a large amount of lipid and cholesterol
266 biosynthesis. De novo biosynthesis of fatty acids (integral building blocks of lipids) and
267 cholesterol is crucially important for SCs to initiate myelination and to grow a myelin sheath
268 (*48-51*). YAP/TAZ may regulate these pathways, as suggested by reduced mRNA expression in
269 *Yap/Taz* cDKO of SREBPs TFs (Sterol regulatory element binding proteins) and their target

270 enzymes involved in lipid/cholesterol biosynthesis (*14, 15*). We therefore investigated, at the
271 protein level, whether TEAD1 and YAP/TAZ are required for fatty acid and/or cholesterol
272 synthesis. To test this premise, we examined expression of SREBP1 and its target SCD1
273 (Stearoyl-CoA desaturase-1), which upregulates fatty acid synthesis, and of SREBP2 and its
274 targets HMGCR (HMG-CoA reductase), FDPS (Farnesyl Diphosphate Synthase) and IDI1
275 (Isopentenyl-diphosphate delta isomerase 1), which upregulate cholesterol synthesis (*51, 52*).
276 Because SREBP pathways are upregulated early postnatally for myelination in WT SNs, their
277 upregulation may simply be delayed in developmentally delayed *Tead1* cKO. We therefore
278 investigated SREBP pathways both at P8 and P40 in WT and *Tead1* cKO mice. Western blot
279 analysis showed that SREBP1 and SCID1 expression in cKO SNs was not significantly affected
280 by loss of TEAD1 at either P8 or P40 (Figure 6A). In contrast to SREBP1, SREBP2 was ~50%
281 reduced in *Tead1* cKO at both P8 and P40. Despite marked reduction in SREBP2, HMGCR was
282 not reduced at P8 or P40. However, both FDPS and IDI1 levels were greatly reduced at both P8
283 and P40 (Figure 6A).
284 It is possible that HMGCR was not reduced in cKO due to TEAD1 redundancy and
285 compensation by other TEADs. If so, then HMGCR levels should be reduced in *Yap/Taz* cDKO,
286 because YAP/TAZ are the primary partners for all TEADs (*24, 32*). To test this idea, we
287 examined SREBP pathways in *Yap/Taz* cDKO SNs at P60 because developmental delay is
288 greater in *Yap/Taz* cDKO than in *Tead1* cKO SNs (*13*). We found that, as in *Tead1* cKO,
289 SREBP1 and SCD1 levels were not noticeably reduced by the loss of YAP/TAZ in cDKO
290 (Figure 6B), suggesting that YAP/TAZ and TEAD1 do not directly affect fatty acid synthesis.
291 Unlike in *Tead1* cKO, levels of SREBP2 were not markedly reduced in Yap/Taz cDKO. As in
292 *Tead1* cKO, however, HMGCR levels were not reduced in Yap/Taz cDKO, whereas levels of
293 FDPS and IDI1 were greatly reduced (Figure 6B). These results therefore suggest that
294 YAP/TAZ-TEAD1 transcriptional complex selectively upregulates IDI1 and FDPS, contributing
295 to cholesterol biosynthesis. Together with the lack of synthesis of myelin proteins, this reduction
296 in cholesterol biosynthesis may prevent myelin formation and growth in *Tead1* cKO.
297
298 **Loss of TEAD1 in adult Schwann cells modestly affects myelin maintenance**
299 Because TEAD1 regulates myelination and Remak bundle formation during
300 development, we next investigated its role in myelin and Remak bundle maintenance in adults.

301 We first verified efficient deletion of TEAD1 in almost all SCs of *Tead1* iKO (Figure 1B).
302 Unlike *Yap/Taz* iDKO mice (*13*), *Tead1* iKO mice appeared normal 2 weeks after tamoxifen
303 administration and continued to survive without obvious signs of peripheral neuropathy up to 5
304 months post-tamoxifen, the longest time of observation (Figure 7A). Analysis of iKO SNs
305 between 3 to 5 months post-tamoxifen revealed that they were grossly normal. However, we
306 occasionally observed large axons undergoing demyelination or completely demyelinated
307 (Figure 7B). Unlike *Yap/Taz* iDKO mice, which frequently exhibited segmental demyelination
308 and markedly reduced NCV (*13*), NCV of these iKO mice did not significantly differ from that
309 of WT (Figure 7C). Therefore, loss of TEAD1 alone in adult SCs evoked only modest
310 demyelination that does not cause significant functional impairment.
311
312 **TEAD1 is required for maintaining structural integrity of Remak bundles**
313 Next, we examined Remak bundles in these mice. As in WT SNs, C-fibers in WT mice
314 were individually ensheathed by SC cytoplasm. In contrast, in *Tead1* iKO, many c-fibers in most
315 Remak bundles were not separated by SC cytoplasm (Figure 7D). Furthermore, some Remak
316 bundles were abnormally myelinated, as in *Tead1* cKO SNs (Figure 7E). Thus, TEAD1 is
317 required for formation as well as maintenance of Remak bundles.
318
319 **TEAD1 is dispensable for YAP/TAZ to maintain Krox20, FDP and IDI1 expression**
320 To investigate why the demyelinating phenotype of *Tead1* iKO is much milder than that
321 of *Yap/Taz* iDKO, we first investigated expression of Krox20 which is required for myelin
322 maintenance (*7*). We previously observed that Krox20 is markedly downregulated in *Yap/Taz*
323 iDKO SCs, which correlated with frequent segmental demyelination and markedly reduced NCV
324 (*13*). As a control, we injected *PLP-CreER; Yap*$^{fl/fl}$*; Taz*$^{fl/fl}$ mice with tamoxifen and reproduced
325 our previous result: Krox20 was dramatically downregulated in most *Yap/Taz* iDKO SCs only 2
326 weeks post-tamoxifen (Figure 7F). In contrast, in *Tead1* iKO, Krox20 expression was
327 indistinguishable from WT even at 6 weeks post-tamoxifen (Figure 7G). We then investigated
328 Oct6 expression, because aberrant overexpression of Oct6 in the presence of Krox20 inhibits
329 myelination (*46*). Unlike in *Yap/Taz* iDKO SNs (*13*), however, Oct6 was not elevated in *Tead1*
330 iKO SNs (Figure 7H). Therefore, TEAD1 is dispensable for maintaining Krox20 expression in
331 myelinating SCs, consistent with the only modest demyelinating phenotype of *Tead1* iKO.

332 Next, we investigated SREBP pathways, which are required for developmental
333 myelination (*50, 51*). Whether these pathways are also involved in myelin maintenance has not
334 been studied. We first assessed the effects of acute loss of YAP/TAZ on these pathways in adult
335 SCs. Western blotting of WT and *Yap/Taz* iDKO SN lysates showed that the SREBP1 pathway,
336 or expression of SREBP2 and HMGCR in the SREBP2 pathway, was unaffected in *Yap/Taz*
337 iDKO (Figure 7I). However, FDPS and IDI1 levels were significantly downregulated in *Yap/Taz*
338 iDKO (Figure 7I), recapitulating the effect of developmental loss of YAP/TAZ on these proteins
339 (Figure 6B). Therefore, the acute downregulation of these key enzymes for cholesterol
340 biosynthesis correlates with the acute demyelination previously observed in *Yap/Taz* iDKO mice.
341 This result suggests that YAP/TAZ maintain myelination through both myelin gene expression
342 and the cholesterol biosynthesis pathway.
343 Western blotting of *Tead1* iKO SN lysates, 6 weeks post-tamoxifen, revealed that the
344 SREBP pathways were not significantly affected by loss of TEAD1 (Figure 7J), unlike *Tead1*
345 cKO in which FDPS and IDI1 were markedly downregulated. This result correlated with the
346 modest effect of loss of TEAD1 on myelin maintenance, suggesting that TEAD1 is largely
347 dispensable for cholesterol synthesis in adult SCs.
348
349 **TEAD1 is required for myelination of regenerating axons after nerve injury**.
350 Next, we investigated whether TEAD1 is required for axon regeneration and
351 remyelination after nerve injury. We previously showed that YAP/TAZ are not required for axon
352 regeneration but are necessary for remyelination (*13*). Because *Yap/Taz* iDKO mice die ~2
353 weeks post-injury, it remains possible that remyelination is delayed rather than completely
354 blocked. In contrast, *Tead1* iKO mice are not susceptible to early death. We, therefore, examined
355 them 4 weeks after crushing SN, when hindlimb muscles are fully reinnervated in WT (Figure
356 8A). We first verified efficient deletion of TEAD1 in almost all SCs of *Tead1* iKO mice after
357 nerve crush (Figure 1C). Longitudinal sections of iKO SNs showed numerous TuJ1-labeled
358 axons that regenerated along the distal nerve stump, as in WT SNs (Figure 8B). However, MBP
359 immunoreactivity was markedly reduced in the distal nerve stump of *Tead1* iKO, compared to
360 WT, suggesting that axons regenerated but were not remyelinated. We also found that
361 regenerated axons reached hindlimb muscles and reinnervated neuromuscular junctions (NMJs)
362 in iKO, as in WT (Figure 8C). Moreover, *Tead1* iKO frequently exhibited features of paralyzed

363 muscles, such as axon terminals that grew past the synaptic area, fragmented clusters of
364 acetylcholine receptors (AChRs), and satellite extra-synaptic AChRs (*53*). Semithin and EM
365 analysis confirmed virtual absence of myelination in iKO SNs; although large axons were
366 associated with SCs, they were not myelinated (Figure 8D). Accordingly, electrical stimulation
367 of iKO SNs did not elicit CMAPs or NCV (Figure 8E). Thus, like YAP/TAZ, TEAD1 in SCs is
368 not required for axon regeneration but is required for remyelination after nerve injury.
369 After injury, SCs transdifferentiate into growth-promoting repair SCs, which then
370 proliferate and reach a peak around 3 dpi (*54-56*). Quantitative analysis of SC proliferation at 3
371 dpi by counting $EdU^+/Sox10^+$ SCs showed that a similar percentage of SCs were in S-phase in
372 both WT and *Tead1* iKO SNs (Figure 8F), suggesting that, like YAP/TAZ (*13*), TEAD1 is not
373 required for proliferation of repair SCs. Lastly, we counted $Krox20^+$ and $Oct6^+$ SCs at 4 wpi.
374 Notably, in contrast to *Yap/Taz* iDKO SCs, which fail to upregulate Krox20 after injury (*13*),
375 Krox20 was upregulated in *Tead1* iKO SCs, as in WT SCs (Figure 8G). Furthermore, Oct6 was
376 aberrantly elevated in *Tead1* iKO SCs, like in *Tead1* cKO SCs during development (Figure 8H).
377 These results suggest that, similar to developmental myelination, remyelination requires TEAD1
378 for Oct6 downregulation and for Krox20 to upregulate myelin proteins. Additionally, almost
379 complete absence of remyelination at 4 wpi highlights that TEAD1 is crucial for functional
380 regeneration of peripheral nerves.
381
382 **DISCUSSION**
383 The present study conclusively establishes TEAD1 as a crucial TF that partners with YAP/TAZ
384 to mediate myelin formation, growth, and regeneration. TEAD1 promotes myelination by dually
385 regulating SC proliferation, by enabling induced Krox20 to upregulate myelin proteins, and by
386 upregulating cholesterol biosynthetic enzymes. Our findings also suggest that other TEADs play
387 redundant and opposing roles in SCs, and that TEAD1 is critical in the proper formation and
388 maintenance of Remak bundles.
389
390 **Unique, redundant, and opposing roles of TEAD1**
391 Although SCs express all four TEADs, *Tead1* cKO mice grossly phenocopies *Yap/Taz* cDKO
392 mice. They exhibit abnormal SC proliferation, delayed radial sorting, blocked myelin formation
393 and remyelination, and normal axon regeneration. Furthermore, *Tead1* cKO mice, like *Yap/Taz*

394 cDKO, are defective in regulating Oct6, Krox20, myelin proteins, and enzymes that synthesize
395 cholesterol. These similarities show that YAP/TAZ regulate both SC proliferation and
396 differentiation, the two opposing processes crucial for myelination, by partnering mainly with
397 TEAD1 at least for developmental myelination and remyelination after injury.
398
399 We also observed multiple differences between *Tead1* cKO and *Yap/Taz* cDKO mutants. Unlike
400 *Yap/Taz* cDKO, *Tead1* cKO initiates myelin formation in some developing axons and maintain
401 myelination in most axons but fails to remyelinate almost all regenerating axons. Additionally, in
402 *Tead1* cKO, Krox20 are upregulated and a large excess of SCs is generated. These differences
403 are likely due to stage-dependent redundancy and opposing roles of TEADs. Consistent with this
404 idea, YAP/TAZ functionally associate with TEAD2, 3 or 4, or an unrelated TF (*57*), in the
405 absence of TEAD1. Loss of TEAD1 does not affect nuclear localization of YAP/TAZ, which
406 depends mainly on interactions with TEADs (*27-30*). Our data and the results of others suggest
407 that TEAD1-4 are all co-expressed in SCs through multiple stages of nerve development,
408 homeostasis and after injury (*13, 34, 37*). Notably, nuclear retention of YAP/TAZ occurs in
409 *Tead1* cKO when TEAD1 has a unique role in SCs (i.e., when *Tead1* cKO SCs fail to form and
410 re-form myelination). Therefore, other TEADs can retain nuclear YAP/TAZ, thereby supporting
411 transcriptional activity of YAP/TAZ, but cannot substitute for some or most of its functions with
412 TEAD1 in a stage-dependent manner.
413
414 It is also notable that, like YAP/TAZ, the unique roles of TEAD1 change dynamically in
415 successive steps of myelination, even though other TEADs are present. Thus, TEAD1 is
416 uniquely required for timely proliferation of SCs during radial sorting; uniquely opposes SC
417 proliferation to promote cell-cycle exit after radial sorting; redundantly promotes upregulation of
418 Krox20; and then uniquely promotes upregulation of myelin proteins and cholesterol
419 biosynthetic enzymes. Such unique and redundant roles for TEAD1 in the presence of other
420 TEADs are supported by cell-based transcription assays, in which YAP-TEAD4 can substitute
421 for YAP-TEAD1 in upregulating transcription from the Krox20 promoter, but not from the MPZ
422 intronic enhancer (*37*). Our data also show that even when TEAD1 is largely redundant because
423 other TEADs are present and can functionally substitute for TEAD1, such as in myelin
424 maintenance, YAP/TAZ preferentially bind to TEAD1. This situation resembles the dynamic

425 function of TEADs in cortical development, another multi-step differentiation program. As in
426 nerve development, multiple TEADs (TEAD1-3) are co-expressed throughout cortical
427 development. Depending on the differentiation stage, TEAD1 uniquely promotes proliferation,
428 redundantly promotes proliferation with TEAD2 and 3, or redundantly promotes differentiation
429 with TEAD3, when it is opposed by TEAD2 (*33*).
430
431 As *Yap/Taz* cDKO SCs arrest at the promyelination stage, we were unable to investigate the role
432 of YAP/TAZ in myelin sheath growth (*13*). In contrast, some *Tead1* cKO SCs can myelinate but
433 fail to grow myelin sheaths proportional in size to axon diameter. Importantly, such myelinating
434 SCs apparently lack TEAD1 because TEAD1 deletion is extremely efficient in *Tead1* cKO mice.
435 Support for a role of TEADs in the regulation of myelin sheath thickness comes from a study of
436 TEAD4 cKO mice, in which SCs lacking TEAD4 gradually upregulate myelin protein
437 expression, resulting in adult mice with abnormally thick myelin (*34*). Therefore, TEADs 1 and 4
438 oppose each other in the regulation of myelin sheath growth. Likewise, they may oppose each
439 other in the regulation of SC proliferation, resulting in a large excess of SCs we observed in P22
440 and P50 *Tead1* cKO.
441
442 **TEAD1 regulation of Krox20 and myelin gene expression**
443 Previous work suggests that YAP/TAZ-TEAD1 promote myelination in part through direct
444 upregulation of Krox20 (*13, 15*). Unlike *Yap/Taz* cKO mice, *Tead1* cKO mice upregulate
445 Egr2/Krox20, but they fail to upregulate myelin proteins and cholesterol biosynthetic enzymes.
446 Our findings extend previous work to suggest that TEAD1 functions redundantly in direct
447 upregulation of Krox20, but that its function is required for upregulated Krox20 to promote
448 myelination. Krox20 activity may be repressed in *Tead1* cKO by Oct6, which remains
449 abnormally elevated. In support of this possibility, persistently elevated Oct6 overrides Krox20
450 to inhibit myelin gene expression (*46, 58*). Other mice with defective lipid biosynthesis and a
451 phenotype like *Tead1* cKO also have abnormally elevated Oct6 after Krox20 upregulation (*49,*
452 *59*). An alternative or additional possibility is that a transcriptional co-activator that synergizes
453 with Krox20 is absent in *Tead1* cKO SCs. We suggest that TEAD1 itself may function as such a
454 factor. Supporting this idea are reports that gene regulatory elements function by co-binding
455 several TFs, which synergistically activate transcription (*60, 61*), as at the Krox20 MSE

456 (Myelinating Schwann cell element) which is the enhancer responsible for Krox20 expression (*9,*
457 *11, 13, 62*). Krox20 synergizes with Sox10 to activate myelin genes (*63*) and with SREBP to
458 activate lipid biosynthesis genes (*52*). Like Krox20, TEAD1 can directly promote transcription
459 from PMP22 and MPZ myelin gene enhancers (*18, 37*). A consistent finding of the present work
460 is that functional Krox20 is insufficient to drive myelin/cholesterol gene expression in the
461 absence of TEAD1. Alternatively, or additionally, TEAD1 may also function indirectly by
462 upregulating co-factors, such as SREBP2, which is reduced in *Tead1* cKO. Notably, lipid
463 biosynthesis is necessary to downregulate Oct6 and upregulate myelin gene transcription during
464 developmental myelination (*50, 51*). An interesting possibility, therefore, is that YAP/TAZ-
465 TEAD1 and Krox20 may cooperatively downregulate Oct6 and upregulate myelin gene
466 expression at least in part by promoting lipid biosynthesis.
467
468 **YAP/TAZ-TEAD1 regulation of cholesterol biosynthesis**
469 SREBP1 levels are not altered in *Tead1* cKO or *Yap/Taz* cDKO, suggesting that fatty acid
470 synthesis is not directly regulated by YAP/TAZ or TEAD1. We did not observe downregulation
471 of HMGCR in *Tead1* cKO or *Yap/Taz* cDKO mice at P8 or P40, which contradicts the report of
472 reduced mRNA expression of HMGCR in *Yap/Taz* mutants at P3 and P5 (*14, 15*); we suggest
473 this difference is due to developmental delay in *Tead1* cKO and *Yap/Taz* cDKO. However,
474 marked downregulation of IDI1 and FDPS in *Tead1* cKO, *Yap/Taz* cDKO, and *Yap/Taz* iDKO
475 suggests that cholesterol biosynthesis is defective in these mutants. In support of this notion, SC-
476 selective deletion of SCAP (SREBP cleavage activation protein), which is required to produce
477 active SREBP1 and SREBP2 (*51*), or of Squalene synthase, an essential enzyme in cholesterol
478 biosynthesis (*50*), evokes phenotypes which are remarkably similar to those of *Tead1* cKO mice:
479 both mutants have an increased number of SCs, a severe delay at the promyelination stage, and
480 persistently thin myelin. In addition, in SCAP cKO, Oct6 is upregulated continuously and
481 Squalene synthase cKO fails to upregulate myelin gene transcription, resulting in severely
482 reduced MBP, MPZ, and PMP22 protein levels.
483
484 How might YAP/TAZ-TEAD1 regulate IDI1 and FDPS? Multiple studies show that YAP/TAZ
485 can activate the mTORC1 pathway (*64, 65*), and IDI1 and FDPS levels are reduced in Raptor
486 cKO SNs (*49*). Furthermore, the Raptor cKO phenotype is like that of *Tead1* cKO, exhibiting an

487 increased number of SCs, normal upregulation of Krox20, persistent upregulation of Oct6, delay
488 at the promyelination stage, and thin myelin. However, HMGCR protein levels are reduced, and
489 aberrant upregulation of Oct6 is transient (*49*). Furthermore, after nerve injury, formation of
490 repair SCs is delayed in Raptor mutants (*66*), unlike TEAD1 and YAP/TAZ mutants. These
491 differences suggest that YAP/TAZ-TEAD1 are not directly upstream of mTORC1. Another
492 possibility is that YAP/TAZ-TEAD1 may directly regulate transcription of IDI1 and FDPS
493 genes. Such direct regulation of cholesterol biosynthetic enzymes has been observed for other
494 TFs in SCs (*52, 67*).
495
496 **TEAD1 regulation of Remak bundles**
497 In both *Tead1* cKO and iKO mice, there is defective ensheathment of C-fibers by SCs in Remak
498 bundles, which are occasionally thinly myelinated. This phenotype is distinct from those mutants
499 in which SCs surround and sometimes myelinate bundles filled with mixed-caliber axons, which
500 are considered radial sorting defects (*44*). Remak bundles can myelinate abnormally in WT SNs
501 during early postnatal development, but this defect is corrected and does not persist in adults
502 (*68*). Therefore, the defective Remak bundles that we observed in *Tead1* cKO are not due to
503 developmental delay, and the defects found in adult *Tead1* iKO appear unusual.
504
505 Remak bundles form normally at P60 in *Yap/Taz* cDKO, although many large bundles containing
506 mixed caliber axons are present during development (*13*). The difference between *Tead1* and
507 *Yap/Taz* mutants is supported by the presence of TEAD1 and absence of YAP/TAZ in non-
508 myelinating SC nuclei (*13*). Notably, defective SC ensheathment of C-fibers and myelinated
509 Remak bundles is observed in various SC developmental mutants, including those with defective
510 SC basal lamina (*68*) and overexpression of NRG1-IIIb in axons (*69*). Therefore, it is possible
511 that TEAD1 mediates extracellular signaling from the SC basal lamina and/or axons that is
512 responsible for forming and maintaining proper association of SCs with C-fibers. Notably, SC
513 ensheathment of C-fibers is required for normal NCV (*70*), and NCV with tg-NRG1-IIIb Remak
514 bundles is reduced compared to WT (*69*). Future studies will address NRG1 signaling and NCV
515 in cKO and iKO mice lacking TEAD1 and/or other TEADs.
516
517 **MATERIALS AND METHODS**

518

519 **Animals**

520 All surgical procedures and animal maintenance complied with the National Institute of Health
521 guidelines regarding the care and use of experimental animals and were approved by the
522 Institutional Animal Care and Use Committee of Temple University, Philadelphia, PA, USA.
523 Generation and genotyping of mice carrying targeted loxP sites in the *Tead1* gene have been
524 described previously (*39*). Targeted ablation of *Tead1* in Schwann cells of embryonic mice was
525 achieved by crossing *Tead1*$^{fl/fl}$ mice with mice transgenic for *Cre* driven by the *Mpz* promoter
526 (*Tead1* cKO mice). Targeted ablation of *Tead1* in Schwann cells of adult mice was by crossing
527 *Tead1*$^{fl/fl}$ mice with mice transgenic for the inducible Cre recombinase *Cre-ERT2* under control
528 of the *Plp1* promoter (*Tead1* iKO mice). Control mice contained floxed *Tead1* alleles but were
529 not transgenic for *Cre* or *Cre-ERT2*. *Mpz-cre*;*Yap*$^{fl/fl}$; *Taz*$^{fl/fl}$ (*Yap/Taz* cDKO) and *Plp1-creERT2*;
530 *Yap*$^{fl/fl}$; *Taz*$^{fl/fl}$ (*Yap/Taz* iDKO) mice used in this study were generated and genotyped as
531 described previously (*13*). Both male and female mice were used in all experiments and were
532 maintained on the C57BL/6 background.

533

534 **Tamoxifen administration**

535 Tamoxifen was prepared and injected into 6–8-week-old *Tead1* or *Yap/Taz* mutant mice as
536 previously described (*13*). A 10 mg/ml solution of tamoxifen was made in 10:1 sunflower oil:
537 100% ethanol. This solution was injected intraperoneally at a concentration of 0.2 mg/g body
538 weight. Injection was once daily for 5 days, followed by a 2-day break, then once daily for 5
539 consecutive days.

540

541 **Nerve crush**

542 Sciatic nerves of right hindlimbs were crushed 24 h after the final tamoxifen injection, as
543 described previously (*17, 71*). A small skin incision was made in the posterior thigh and calf of
544 the animals anesthetized by isoflurane. The sciatic nerve was crushed with a fine forceps (#5) for
545 10 seconds (3X) adjacent to the sciatic notch. The crush site was marked using charcoal-coated
546 forceps, and the wound was closed. To identify proliferating Schwann cells, we intraperitoneally
547 injected EdU (80 μg/g) eighty minutes before euthanasia, as previously described (*13*).

548

549 **Western blotting and immunoprecipitation**

550 After removal of epineurium and perineurium, sciatic nerves were snap-frozen in liquid nitrogen
551 and stored at -80ºC. For Western blotting, sciatic nerves were lysed in RIPA buffer (25 mM Tris
552 pH 7.5, 150 mM NaCl, 1% Triton X-100, 0.5% sodium deoxycholate, 1 mM EDTA, 0.1% SDS);
553 for immunoprecipitation, lysis was in co-IP buffer (50 mM Tris pH 8.0, 150 mM NaCl, 0.5%
554 Triton X-100, 10% glycerol, 1 mM EDTA), both containing protease and phosphatase inhibitors.
555 Lysis was for 40 minutes on ice, followed by microcentrifugation at 14,000 rpm for 20 minutes.
556 Protein concentration was determined using the BCA assay (ThermoFisher).

557 Immunoprecipitation was overnight at 4ºC, followed by 1 hour with protein A sepharose
558 (pre-blocked with 1% BSA), both with constant rotation. Lysates and immunoprecipitated
559 complexes in 1x Laemmli buffer were resolved on 8 or 10% SDS-PAGE gels, transferred to
560 nitrocellulose, and blotted with the appropriate antibodies. Primary antibodies were used at the
561 following concentrations for Western blots or immunoprecipitations: rabbit anti-Krox20
562 (Covance; 1:400), rabbit anti-Oct6 (Abcam ab126746; 1:1000), mouse anti-Myelin Basic Protein
563 (Covance SMI94; 1:1000), mouse anti-beta actin (SIGMA-Aldrich A5441; 1:5000), rabbit anti-
564 TEAD1 (Cell Signaling D9X2L, #12292; 1:1000), rabbit anti-TEAD2 (Novus Biologicals,
565 #NBP3-05267; 1:1000), rabbit anti-TEAD3 (Cell Signaling #13224; 1:1000), rabbit anti-TEAD4
566 (Santa Cruz, #sc-101184; 1:1000), rabbit anti-pan-TEAD (Cell Signaling, #13295; 1:1000),
567 rabbit anti-YAP/TAZ (Cell Signaling D24E4, #8418; 1:1000, 1:100 for immunoprecipitations),
568 rabbit anti-phospho-YAP(Ser127) (Cell Signaling D9W2I #13008; 1:1000), rabbit anti-phospho-
569 YAP(Ser397) (Cell Signaling D1E7Y #13619; 1:1000), rabbit-anti-MPZ (Cell Signaling #57518;
570 1:1000), mouse anti-SREBP1 (Novus Biologicals, #NB600-582; 1:1000), rabbit anti-SCD1 (Cell
571 Signaling, #2794; 1:1000), rabbit anti-SREBP2 (Bethyl laboratories, #A303-125A), rabbit anti-
572 HMGCR (Novus Biologicals, #NBP2-66888; 1:1000), rabbit anti-FDPS (Proteintech, #16129-1-
573 AP; 1:1000), rabbit anti-IDI1 (Proteintech, #11166-2-AP; 1:1000). Control whole rabbit IgG for
574 immunoprecipitations was from Jackson Laboratories (011-000-003) and was used at 1μg/ml,
575 which was several-fold greater than all other antibodies used for immunoprecipitations.
576 Secondary antibodies for Western blotting were HRP-linked sheep anti-mouse IgG and donkey
577 anti-rabbit (both GE Healthcare; 1:5000) and HRP-linked mouse anti-rabbit, light-chain specific
578 (Jackson ImmunoResearch 211-032-171; 1:20,000). Blots were developed using ECL, ECL Plus
579 (GE Healthcare) or Odyssey (LiCor).

580

581 **Immunohistochemistry, confocal and widefield fluorescence microscopy**

582 For immunostaining, sciatic nerves were removed and immediately fixed in 4%
583 paraformaldehyde in PBS for 1 hr. on ice. Nerves were washed 3 times in PBS, then stored in
584 15% sucrose in PBS overnight at 4°C for cryoprotection. Nerves were frozen-embedded in
585 cryoprotectant medium (Thermo Fisher Scientific, Waltham, MA) in isomethylbutane at -80°C.
586 7-10 μm sections from the nerves were cut using a cryostat (Leica Microsystems, Germany) and
587 collected directly onto glass slides. For immunolabeling, nerve sections were rehydrated in PBS,
588 permeabilized in 0.5% Triton/PBS for 20 min, washed with PBS, then blocked in 2% bovine
589 serum albumin (BSA) in PBS for 1 hr. Sections were incubated with primary antibodies in
590 blocking buffer overnight at 4°C in a hydrated chamber, washed with PBS, and incubated with
591 secondary antibodies in blocking buffer for 2 hrs. at room temperature. Sections were washed
592 with PBS, stained with DAPI for 10 min, and mounted with Vectashield mounting medium
593 (Vector Labs, Burlingame, CA).

594 Primary antibodies were used at the following concentrations for immunostaining of
595 cryosections: guinea pig anti-Sox10 (kind gift from Michael Wegner, University of Erlangen,
596 Bavaria, Germany; 1:1000), rabbit anti-Krox20 (Covance; 1:400), rabbit anti-Oct6 (Abcam
597 ab31766; 1:800), rabbit anti-Ki67 (Novocastra NCL-Ki67p; 1:200), rabbit anti-Neurofilament
598 200 (SIGMA-Aldrich N4142; 1:500), mouse anti-Neurofilament (Covance SMI 312; 1:1000),
599 mouse anti-Tubulin β3 (clone Tuj1, Covance #MMS-435P; 1:1000), mouse anti-SV2
600 (Developmental Studies Hybridoma Bank, Iowa; 1:10), rabbit anti-S100 (DAKO; 1:600), mouse
601 anti-Myelin Basic Protein (Covance SMI 94; 1:2000), rabbit anti-TEAD1 (Cell Signaling
602 D9X2L, #12292; 1:200), rabbit anti-pan-TEAD (Cell Signaling D3F7L, #13295; 1:200), rabbit
603 anti-YAP/TAZ (Cell Signaling D24E4, #8418; 1:200).

604 For immunostaining of extensor digitorum longus (EDL) and soleus muscles, mice were
605 perfused with 4% paraformaldehyde, and the muscles removed and post-fixed for 20 mins at
606 room temperature. Muscles were then incubated for 15 minutes with rhodamine-conjugated α-
607 bungarotoxin (Invitrogen, Carlsbad, CA), permeabilized in –20°C methanol for 5 min, and
608 blocked for 1 hr. in PBS containing 0.2% Triton and 2% BSA. The muscles were subsequently
609 incubated overnight at 4ºC in a cocktail of primary antibodies diluted in the blocking solution.
610 Axons and nerve terminals were labeled with mouse monoclonal antibodies to neurofilaments

611 (SMI 312; Sternberger Monoclonals, Baltimore, MD) and to a synaptic vesicle protein, SV2
612 (Developmental Studies Hybridoma Bank, Iowa City, IA). Schwann cells were labeled with
613 rabbit anti-cow S-100 polyclonal antibody (Dako, Carpentaria, CA). After incubation with the
614 primary antibodies, muscles were rinsed in PBS and incubated with secondary antibodies in the
615 blocking solution, for 1 hr. at room temperature. The muscles were then rinsed in PBS and
616 prepped for whole-mount by peeling the top layer of muscle fibers using microscissors and
617 forceps, as previously described (*71*). The resulting "muscle fillets" were mounted on a slide and
618 coverslipped.
619 Conventional fluorescence microscopy was performed using Olympus BX53 and Zeiss
620 Axio Imager 2 microscopes. Images were captured using Hamamatsu ORCA R2 C10600 or
621 Zeiss Axiocam HRm Rev 3 digital cameras, respectively, and Metamorph software. For confocal
622 microscopy, we used a Leica SP8 confocal microscope, with either a 40x 1.3 NA or 63x 1.4 NA
623 objective and Leica proprietary software. Acquired stacks were assembled using the maximum
624 projection tool, and figures were prepared using Adobe Photoshop.
625
626 **Electron microscopy, histology, and morphometry**
627 Mice were perfused intravascularly with 2.5% glutaraldehyde and 4% paraformaldehyde in 0.1M
628 cacodylate buffer pH 7.4. Sciatic nerves were removed and incubated in the same buffer for 90
629 minutes at room temperature, then overnight at 4°C. Specimens were post-fixed for 1 hr. with
630 OsO_4, dehydrated, then embedded in araldite. Semi-thin (0.5 μm) and ultrathin (70 nm) sections
631 were cut using an ultramicrotome and stained with toluidine blue or uranyl acetate and lead
632 citrate, respectively. Semi-thin sections were examined using bright field on an Olympus BX53
633 microscope, and images were captured using Hamamatsu ORCA R2 C10600 digital camera and
634 Metamorph software. For analysis of the number of myelin profiles in control vs mutant sciatic
635 nerves, semi-thin sections from proximal-, mid- and distal regions of the sciatic nerve were
636 taken, and 2 non- overlapping images of each section were obtained using the 60x objective. For
637 electron microscopy, stained ultrathin sections were examined using a JEOL 1010 electron
638 microscope fitted with a Hamamatsu digital camera and AMT Advantage image capture
639 software.
640
641 **Proliferation assays**

642 The percentage of Schwann cells in S-phase was measured by EdU incorporation. Mice were
643 injected intraperitoneally and subcutaneously with 80 μg/ g body weight of EdU dissolved in
644 PBS. Eighty minutes later, mice were sacrificed, and sciatic nerves removed and fixed for 1 hr.
645 in 4% paraformaldehyde; longitudinal 7μm cryosections were used for analysis. EdU
646 incorporation was identified using the Click-iT EdU Alexa Fluor 555 labeling kit (Molecular
647 Probes); the recommended protocol was followed, and labeling was for 1 hr. After EdU labeling,
648 sections were immunostained with anti-Sox10 to identify Schwann cells. The percentage of
649 Schwann cells (Sox10+ nuclei) that were EdU+ was determined by counting confocal images
650 using ImageJ software.
651
652 **Electrophysiology**
653 The procedure for measuring nerve conduction velocity was an adaption of a previously used
654 protocol (*72*). Mice were deeply anesthetized, and hair was completely removed from the
655 hindquarters. A 27g percutaneous needle electrode was inserted subcutaneously over the femur
656 to stimulate the sciatic nerve at two locations: one proximal to the spinal cord, at the hip joint,
657 and the other 1cm distal to this site. The stimulation reference electrode (26G percutaneous
658 needle) was inserted over the back. Bipolar EMG electrodes were inserted subcutaneously in the
659 digital interosseous muscles, to record compound action potentials in response to activation of
660 the sciatic nerve. Stimulation and recording were conducted on both hindlimbs. The muscle
661 response was first tested with single pulses (100 μs duration) to determine the threshold and level
662 of activation producing a stable compound action potential in the muscle. The level of
663 stimulation which produced stable responses was then used for two series of stimulations with 2-
664 20s long trains of biphasic square wave pulses (100 μs duration) delivered at 1-5 Hz. The nerve
665 was rested for 2 minutes between runs. Stimulation was delivered via an isolated pulse stimulator
666 (A-M Systems Model 2100, A-M Systems Inc, Carlsborg, WA). EMG compound muscle action
667 potential (CMAP) responses were recorded with a differential AC amplifier (A-M Systems
668 Model 1700; gain 1k-10k; pass band 10-50 KHz). Data was sampled at 50 KHz using LabVIEW
669 (National Instruments Corporation, Austin, TX) running on a personal computer. Multiple
670 recordings were taken at each location to ensure a minimum of 10 representative responses for
671 each location and animal. Electrophysiological data were analyzed using Igor Pro (Wavemetrics
672 Inc, Lake Oswego, OR).

673

674 **Data Analysis**

675 In each experiment, data collection and analysis were performed identically, regardless of mouse
676 genotype. Data are presented as mean +/- SD. Statistical analysis was done using the student's
677 unpaired t-test for two-group comparisons and analysis of variance (ANOVA) with Tukey's test
678 for multiple comparisons, according to the number of samples and the analysis of mice at
679 multiple ages. Sample sizes were similar to those conventional in the field and are indicated in
680 the main text, methods, or figure legends. A p-value of 0.05 or less was considered statistically
681 significant.

682

683 **SUPPLMENTARY MATERIALS**

684

685 **Supplementary figure 1. Additional semi-thin and TEM images of WT and *Tead1* cKO**

686 **(A)** Representative images of semi-thin sections of various areas of WT and Tead1 cKO SNs at
687 P22 and P50. Scale bar: 20μm

688 **(B)** Representative TEM images of transverse sections of WT and Tead1 cKO SNs at P22 and
689 P50. Scale bar: 1μm (P22 panels), 2μm (P50 panels)

690

691 **Supplementary video 1. A movie showing a P55 WT and two littermates *Tead1* cKO mice**

692

693 **REFERENCES AND NOTES**

694

695 1. K. R. Jessen, R. Mirsky, The origin and development of glial cells in peripheral nerves.
696 *Nat Rev Neurosci* **6**, 671-682 (2005).

697 2. J. L. Salzer, Schwann cell myelination. *Cold Spring Harb Perspect Biol* **7**, a020529 (2015).

698 3. B. Beirowski *et al.*, Metabolic regulator LKB1 is crucial for Schwann cell-mediated axon
699 maintenance. *Nat Neurosci* **17**, 1351-1361 (2014).

700 4. B. L. Harty, K. R. Monk, Unwrapping the unappreciated: recent progress in Remak
701 Schwann cell biology. *Current opinion in neurobiology* **47**, 131-137 (2017).

702 5. S. S. Scherer, L. Wrabetz, Molecular mechanisms of inherited demyelinating neuropathies.
703 *Glia* **56**, 1578-1589 (2008).

704 6. M. Bremer *et al.*, Sox10 is required for Schwann-cell homeostasis and myelin maintenance
705 in the adult peripheral nerve. *Glia* **59**, 1022-1032 (2011).
706 7. L. Decker *et al.*, Peripheral myelin maintenance is a dynamic process requiring constant
707 Krox20 expression. *The Journal of neuroscience : the official journal of the Society for*
708 *Neuroscience* **26**, 9771-9779 (2006).
709 8. M. Finzsch *et al.*, Sox10 is required for Schwann cell identity and progression beyond the
710 immature Schwann cell stage. *J Cell Biol* **189**, 701-712 (2010).
711 9. Y. He *et al.*, Yy1 as a molecular link between neuregulin and transcriptional modulation
712 of peripheral myelination. *Nat Neurosci* **13**, 1472-1480 (2010).
713 10. M. Jaegle *et al.*, The POU proteins Brn-2 and Oct-6 share important functions in Schwann
714 cell development. *Genes Dev* **17**, 1380-1391 (2003).
715 11. S. C. Kao *et al.*, Calcineurin/NFAT signaling is required for neuregulin-regulated Schwann
716 cell differentiation. *Science* **323**, 651-654 (2009).
717 12. N. Le *et al.*, Nab proteins are essential for peripheral nervous system myelination. *Nat*
718 *Neurosci* **8**, 932-940 (2005).
719 13. M. Grove *et al.*, YAP/TAZ initiate and maintain Schwann cell myelination. *Elife* **6**, (2017).
720 14. Y. Poitelon *et al.*, YAP and TAZ control peripheral myelination and the expression of
721 laminin receptors in Schwann cells. *Nat Neurosci* **19**, 879-887 (2016).
722 15. Y. Deng *et al.*, A reciprocal regulatory loop between TAZ/YAP and G-protein Galphas
723 regulates Schwann cell proliferation and myelination. *Nat Commun* **8**, 15161 (2017).
724 16. H. Jeanette *et al.*, YAP and TAZ regulate Schwann cell proliferation and differentiation
725 during peripheral nerve regeneration. *Glia* **69**, 1061-1074 (2021).
726 17. M. Grove, H. Lee, H. Zhao, Y. J. Son, Axon-dependent expression of YAP/TAZ mediates
727 Schwann cell remyelination but not proliferation after nerve injury. *Elife* **9**, (2020).
728 18. C. Lopez-Anido *et al.*, Tead1 regulates the expression of Peripheral Myelin Protein 22
729 during Schwann cell development. *Hum Mol Genet*, (2016).
730 19. P. Topilko *et al.*, Krox-20 controls myelination in the peripheral nervous system. *Nature*
731 **371**, 796-799 (1994).
732 20. N. Le *et al.*, Analysis of congenital hypomyelinating Egr2Lo/Lo nerves identifies Sox2 as
733 an inhibitor of Schwann cell differentiation and myelination. *Proc Natl Acad Sci U S A* **102**,
734 2596-2601 (2005).

735 21. S. W. Jang *et al.*, Locus-wide identification of Egr2/Krox20 regulatory targets in myelin
736 genes. *J Neurochem* **115**, 1409-1420 (2010).
737 22. S. W. Jang, J. Svaren, Induction of myelin protein zero by early growth response 2 through
738 upstream and intragenic elements. *J Biol Chem* **284**, 20111-20120 (2009).
739 23. S. E. LeBlanc, S. W. Jang, R. M. Ward, L. Wrabetz, J. Svaren, Direct regulation of myelin
740 protein zero expression by the Egr2 transactivator. *J Biol Chem* **281**, 5453-5460 (2006).
741 24. Y. Zheng, D. Pan, The Hippo Signaling Pathway in Development and Disease.
742 *Developmental cell* **50**, 264-282 (2019).
743 25. J. H. Xiao, I. Davidson, H. Matthes, J. M. Garnier, P. Chambon, Cloning, expression, and
744 transcriptional properties of the human enhancer factor TEF-1. *Cell* **65**, 551-568 (1991).
745 26. L. Currey, S. Thor, M. Piper, TEAD family transcription factors in development and
746 disease. *Development* **148**, (2021).
747 27. M. Diepenbruck *et al.*, Tead2 expression levels control the subcellular distribution of Yap
748 and Taz, zyxin expression and epithelial-mesenchymal transition. *J Cell Sci* **127**, 1523-
749 1536 (2014).
750 28. J. Kim *et al.*, MAML1/2 promote YAP/TAZ nuclear localization and tumorigenesis. *Proc*
751 *Natl Acad Sci U S A* **117**, 13529-13540 (2020).
752 29. M. Kofler *et al.*, Mediated nuclear import and export of TAZ and the underlying molecular
753 requirements. *Nature communications* **9**, 4966 (2018).
754 30. F. Yao *et al.*, SKP2- and OTUD1-regulated non-proteolytic ubiquitination of YAP
755 promotes YAP nuclear localization and activity. *Nature communications* **9**, 2269 (2018).
756 31. D. Gerber *et al.*, Transcriptional profiling of mouse peripheral nerves to the single-cell
757 level to build a sciatic nerve ATlas (SNAT). *Elife* **10**, (2021).
758 32. J. K. Holden, C. N. Cunningham, Targeting the Hippo Pathway and Cancer through the
759 TEAD Family of Transcription Factors. *Cancers (Basel)* **10**, (2018).
760 33. T. Mukhtar *et al.*, Tead transcription factors differentially regulate cortical development.
761 *Scientific reports* **10**, 4625 (2020).
762 34. X. He *et al.*, A histone deacetylase 3-dependent pathway delimits peripheral myelin growth
763 and functional regeneration. *Nature medicine* **24**, 338-351 (2018).

764 35. T. Wen *et al.*, Transcription factor TEAD1 is essential for vascular development by
765 promoting vascular smooth muscle differentiation. *Cell death and differentiation* **26**, 2790-
766 2806 (2019).
767 36. R. Liu *et al.*, Tead1 is required for perinatal cardiomyocyte proliferation. *PloS one* **14**,
768 e0212017 (2019).
769 37. R. N. Fernando *et al.*, Optimal myelin elongation relies on YAP activation by axonal
770 growth and inhibition by Crb3/Hippo pathway. *Nat Commun* **7**, 12186 (2016).
771 38. C. Lopez-Anido *et al.*, Differential Sox10 genomic occupancy in myelinating glia. *Glia*,
772 (2015).
773 39. T. Wen *et al.*, Characterization of mice carrying a conditional TEAD1 allele. *Genesis (New*
774 *York, N.Y. : 2000)* **55**, (2017).
775 40. M. L. Feltri *et al.*, P0-Cre transgenic mice for inactivation of adhesion molecules in
776 Schwann cells. *Ann N Y Acad Sci* **883**, 116-123 (1999).
777 41. D. P. Leone *et al.*, Tamoxifen-inducible glia-specific Cre mice for somatic mutagenesis in
778 oligodendrocytes and Schwann cells. *Mol Cell Neurosci* **22**, 430-440 (2003).
779 42. A. Beverdam *et al.*, Yap controls stem/progenitor cell proliferation in the mouse postnatal
780 epidermis. *J Invest Dermatol* **133**, 1497-1505 (2013).
781 43. Z. Meng, T. Moroishi, K. L. Guan, Mechanisms of Hippo pathway regulation. *Genes Dev*
782 **30**, 1-17 (2016).
783 44. M. L. Feltri, Y. Poitelon, S. C. Previtali, How Schwann Cells Sort Axons: New Concepts.
784 *Neuroscientist* **22**, 252-265 (2016).
785 45. C. Hindley, A. Philpott, Co-ordination of cell cycle and differentiation in the developing
786 nervous system. *Biochem J* **444**, 375-382 (2012).
787 46. E. J. Ryu *et al.*, Misexpression of Pou3f1 results in peripheral nerve hypomyelination and
788 axonal loss. *J Neurosci* **27**, 11552-11559 (2007).
789 47. T. S. Zorick, D. E. Syroid, A. Brown, T. Gridley, G. Lemke, Krox-20 controls SCIP
790 expression, cell cycle exit and susceptibility to apoptosis in developing myelinating
791 Schwann cells. *Development* **126**, 1397-1406 (1999).
792 48. L. Montani *et al.*, De novo fatty acid synthesis by Schwann cells is essential for peripheral
793 nervous system myelination. *J Cell Biol* **217**, 1353-1368 (2018).

794 49. C. Norrmen *et al.*, mTORC1 controls PNS myelination along the mTORC1-RXRgamma-
795 SREBP-lipid biosynthesis axis in Schwann cells. *Cell Rep* **9**, 646-660 (2014).
796 50. G. Saher *et al.*, Cholesterol regulates the endoplasmic reticulum exit of the major
797 membrane protein P0 required for peripheral myelin compaction. *J Neurosci* **29**, 6094-
798 6104 (2009).
799 51. M. H. Verheijen *et al.*, SCAP is required for timely and proper myelin membrane synthesis.
800 *Proc Natl Acad Sci U S A* **106**, 21383-21388 (2009).
801 52. S. E. Leblanc *et al.*, Regulation of cholesterol/lipid biosynthetic genes by Egr2/Krox20
802 during peripheral nerve myelination. *J Neurochem* **93**, 737-748 (2005).
803 53. M. C. Wright, W. J. Cho, Y. J. Son, Distinct patterns of motor nerve terminal sprouting
804 induced by ciliary neurotrophic factor vs. botulinum toxin. *J Comp Neurol* **504**, 1-16
805 (2007).
806 54. A. Clemence, R. Mirsky, K. R. Jessen, Non-myelin-forming Schwann cells proliferate
807 rapidly during Wallerian degeneration in the rat sciatic nerve. *J Neurocytol* **18**, 185-192
808 (1989).
809 55. K. R. Jessen, R. Mirsky, The repair Schwann cell and its function in regenerating nerves.
810 *J Physiol* **594**, 3521-3531 (2016).
811 56. N. Tricaud, H. T. Park, Wallerian demyelination: chronicle of a cellular cataclysm. *Cell*
812 *Mol Life Sci* **74**, 4049-4057 (2017).
813 57. X. Varelas, The Hippo pathway effectors TAZ and YAP in development, homeostasis and
814 disease. *Development* **141**, 1614-1626 (2014).
815 58. E. S. Monuki, R. Kuhn, G. Lemke, Repression of the myelin P0 gene by the POU
816 transcription factor SCIP. *Mech Dev* **42**, 15-32 (1993).
817 59. D. L. Sherman *et al.*, Arrest of myelination and reduced axon growth when Schwann cells
818 lack mTOR. *The Journal of neuroscience : the official journal of the Society for*
819 *Neuroscience* **32**, 1817-1825 (2012).
820 60. S. Heinz, C. E. Romanoski, C. Benner, C. K. Glass, The selection and function of cell type-
821 specific enhancers. *Nat Rev Mol Cell Biol* **16**, 144-154 (2015).
822 61. B. Ren, F. Yue, Transcriptional Enhancers: Bridging the Genome and Phenome. *Cold*
823 *Spring Harb Symp Quant Biol* **80**, 17-26 (2015).

824 62. J. Ghislain, P. Charnay, Control of myelination in Schwann cells: a Krox20 cis-regulatory
825 element integrates Oct6, Brn2 and Sox10 activities. *EMBO Rep* **7**, 52-58 (2006).
826 63. E. A. Jones *et al.*, Interactions of Sox10 and Egr2 in myelin gene regulation. *Neuron Glia*
827 *Biol* **3**, 377-387 (2007).
828 64. J. K. Hu *et al.*, An FAK-YAP-mTOR Signaling Axis Regulates Stem Cell-Based Tissue
829 Renewal in Mice. *Cell Stem Cell* **21**, 91-106 e106 (2017).
830 65. M. Kim, T. Kim, R. L. Johnson, D. S. Lim, Transcriptional co-repressor function of the
831 hippo pathway transducers YAP and TAZ. *Cell Rep* **11**, 270-282 (2015).
832 66. C. Norrmén *et al.*, mTORC1 Is Transiently Reactivated in Injured Nerves to Promote c-
833 Jun Elevation and Schwann Cell Dedifferentiation. *The Journal of neuroscience : the*
834 *official journal of the Society for Neuroscience* **38**, 4811-4828 (2018).
835 67. M. Kim *et al.*, Maf links Neuregulin1 signaling to cholesterol synthesis in myelinating
836 Schwann cells. *Genes Dev* **32**, 645-657 (2018).
837 68. K. Rasi *et al.*, Lack of collagen XV impairs peripheral nerve maturation and, when
838 combined with laminin-411 deficiency, leads to basement membrane abnormalities and
839 sensorimotor dysfunction. *J Neurosci* **30**, 14490-14501 (2010).
840 69. J. A. Gomez-Sanchez *et al.*, Sustained axon-glial signaling induces Schwann cell
841 hyperproliferation, Remak bundle myelination, and tumorigenesis. *The Journal of*
842 *neuroscience : the official journal of the Society for Neuroscience* **29**, 11304-11315 (2009).
843 70. C. Taveggia *et al.*, Neuregulin-1 type III determines the ensheathment fate of axons.
844 *Neuron* **47**, 681-694 (2005).
845 71. Y. J. Son, W. J. Thompson, Schwann cell processes guide regeneration of peripheral axons.
846 *Neuron* **14**, 125-132 (1995).
847 72. A. Schulz, C. Walther, H. Morrison, R. Bauer, In vivo electrophysiological measurements
848 on mouse sciatic nerves. *J Vis Exp*, (2014).
849
850
851 **ACKNOWLEDGMENTS**
852 We thank members of the Son laboratory for critical reading of the manuscript. We thank Dr.
853 Eric Olson for *Yap* and *Taz* floxed mice, Drs. Ueli Suter and Kelly Monk for Plp-creERT2 mice.

854 Plp-creERT2 mice were generated by Dr. Ueli Suter using a patented Cre-ERT2 construct
855 developed by Dr. Pierre Chambon at GIE-CERBM.

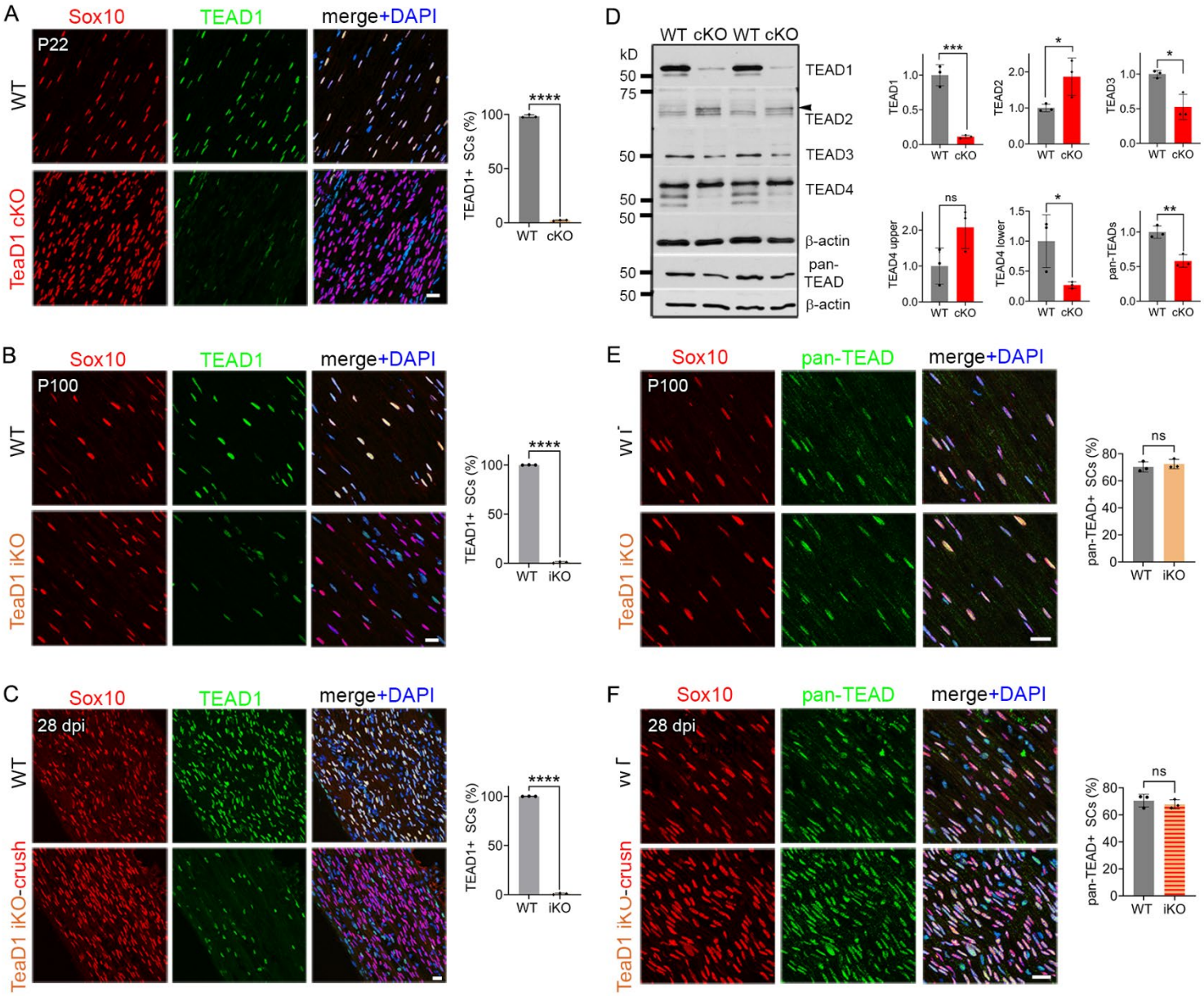

856

857 **Figure 1. Expression of TEADs in Schwann cells (SCs) of WT, *Tead1* cKO, and iKO mice**
858 **(A)** Immunostaining and quantification of TEAD1+ SCs on longitudinal sections of P22 WT and
859 *Tead1* cKO SNs. SC nuclei are identified by Sox10. All cell nuclei are marked by DAPI. n = 3
860 mice per genotype, ****P < 0.0001, Student's unpaired t-test. Scale bar: 20µm

861 **(B)** Immunostaining and quantification of TEAD1+ SCs on longitudinal sections of WT and
862 *Tead1* iKO SNs 3 months after tamoxifen administration. SC nuclei are identified by Sox10. All
863 cell nuclei are marked by DAPI. n = 3 mice per genotype, ****P < 0.0001, Student's unpaired t-
864 test. Scale bar: 20μm
865 **(C)** Immunostaining and quantification of TEAD1+ SCs on longitudinal sections of WT and
866 *Tead1* iKO SNs 28 days after nerve crush. SC nuclei are identified by Sox10. All cell nuclei are
867 marked by DAPI. n = 3 mice per genotype, ****P < 0.0001, Student's unpaired t-test. Scale bar:
868 20μm
869 **(D)** Western blotting of P50 WT and *Tead1* cKO SN lysates with anti-TEAD1, -TEAD2, -
870 TEAD3, -TEAD4, and -pan TEAD. TEAD expression is normalized to that of *β-actin* as an
871 internal control, and WT expression is arbitrarily given the value 1. n = 3 mice per genotype. ns,
872 p > 0.05; *p ≤ 0.05, **p ≤ 0.005, ***p ≤ 0.001, unpaired Student's t-test.
873 **(E)** Immunostaining and quantification of pan-TEAD+ SCs on longitudinal sections of P100 WT
874 and *Tead1* iKO SNs. SC nuclei are identified by Sox10. All cell nuclei are marked by DAPI. n =
875 3 mice per genotype. ns, p > 0.05, Student's unpaired t-test. Scale bar: 20μm
876 **(F)** Immunostaining and quantification of pan-TEAD+ SCs on longitudinal sections of P100 WT
877 and *Tead1* iKO SNs 28 days after nerve crush. SC nuclei are identified by Sox10. All cell nuclei
878 are marked by DAPI. n = 3 mice per genotype. ns, p > 0.05, Student's unpaired t-test. Scale bar:
879 20μm

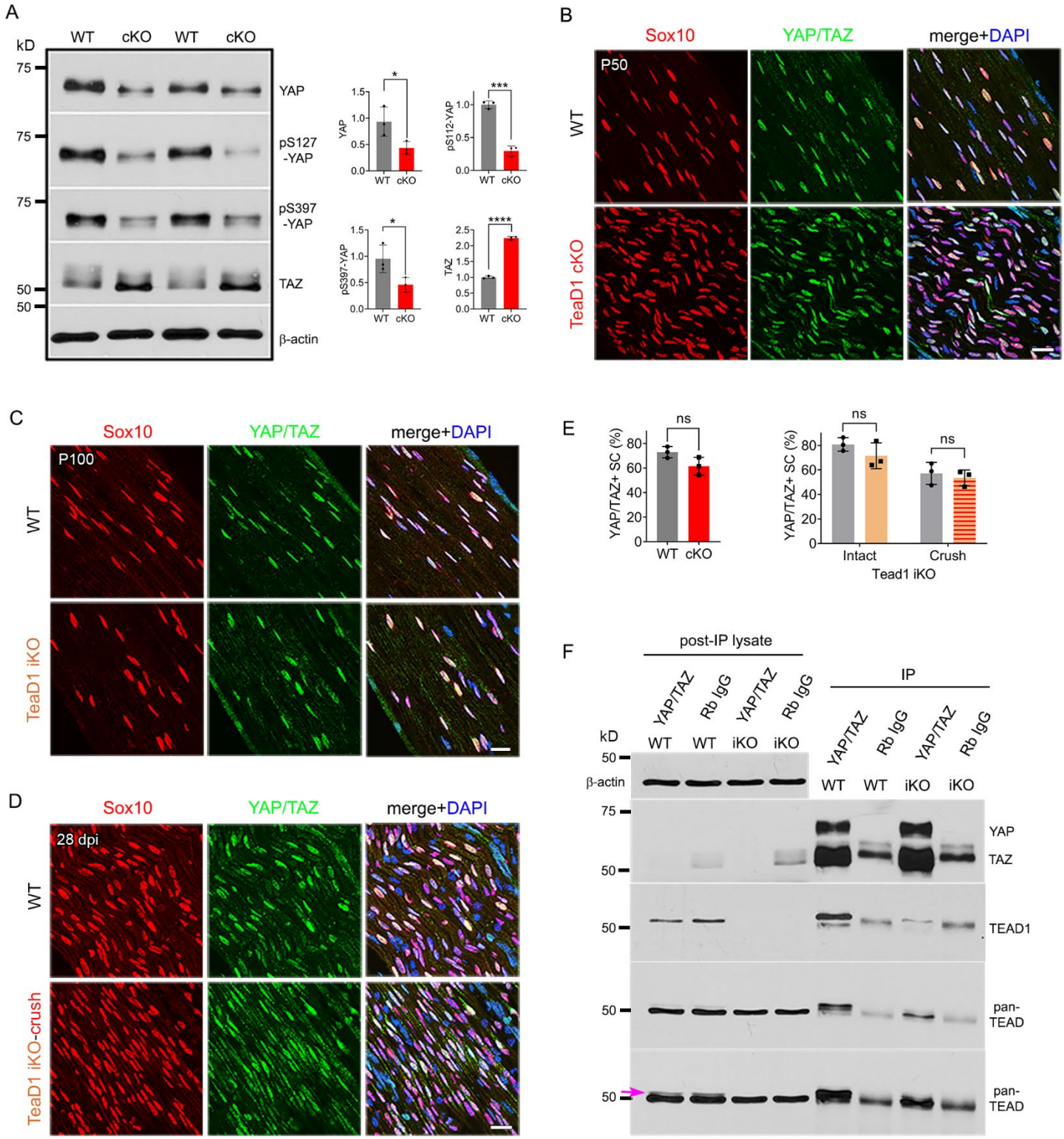

880

881 **Figure 2. YAP/TAZ strongly favor TEAD1 but partner with other TEADs**

882 **(A)** Western blotting of P50 WT and *Tead1* cKO SN lysates with anti-YAP, -phospho-YAPs
883 (Ser127 and Ser397), and -TAZ. YAP/TAZ expression is normalized to that of *β-actin* as an
884 internal control, and WT expression is arbitrarily given the value 1. n = 3 mice per genotype. *p
885 ≤ 0.05, ***p ≤ 0.001, ****P < 0.0001, Student's unpaired t-test.
886 **(B)** Immunostaining of YAP/TAZ+ SCs on longitudinal sections of P50 WT and *Tead1* cKO
887 SNs. SC nuclei are identified by Sox10. All cell nuclei are marked by DAPI. Scale bar: 20μm
888 **(C)** Immunostaining of YAP/TAZ+ SCs on longitudinal sections of P100 WT and *Tead1* iKO
889 SNs. SC nuclei are identified by Sox10. All cell nuclei are marked by DAPI. Scale bar: 20μm
890 **(D)** Immunostaining of YAP/TAZ+ SCs on longitudinal sections of P100 WT and *Tead1* iKO
891 SNs 28 days after nerve crush. SC nuclei are identified by Sox10. All cell nuclei are marked by
892 DAPI. Scale bar: 20μm
893 **(E)** Quantification of YAP/TAZ+ SCs in WT, Tead1 cKO, intact, and injured *Tead1* iKO SNs. n
894 = 3 mice per group. ns, p > 0.05, Student's unpaired t-test.
895 **(F)** Immunoprecipitation of P100 WT and *Tead1* iKO SN lysates with anti-YAP/TAZ and
896 control Rb IgG. Lysate samples, labeled post-IP lysate, were taken from tubes after
897 immunoprecipitated complexes attached to beads had been spun down to assess the efficiency.
898 Immunoprecipitates were blotted for YAP/TAZ, TEAD1, and pan-TEAD. Arrow denotes a faint
899 TEAD1 band revealed by pan-TEAD in WT lysate.
900

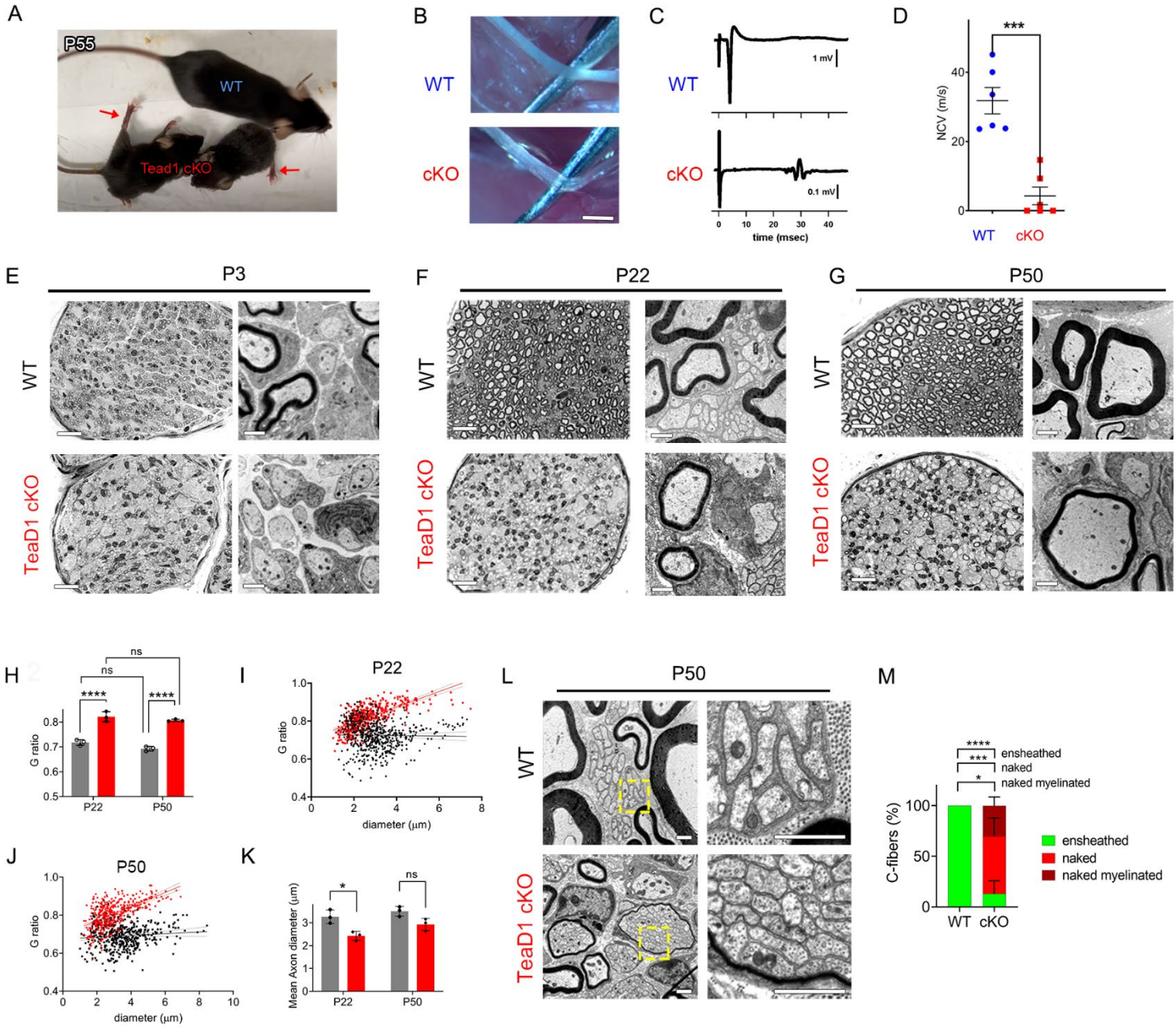

Figure 3. TEAD1 is required for myelin sheath formation and growth

(A) A living control (WT) and two *Tead1* cKO mice from one litter at P55. Arrows point to splayed paralyzed hindlimbs.

(B) Exposed SNs of WT and *Tead1* cKO mice during dissection. Scale bar: 1mm

(C) Representative images of CMAPs generated by stimulation of WT and *Tead1* cKO SNs.

907 **(D)** Quantification of NCV in WT and *Tead1* cKO. n = 6 mice per genotype. ***P < 0.001,
908 Student's unpaired t-test.
909 **(E)** Representative images of semithin (left panels) and TEM (right panels) of transverse sections
910 of WT and *Tead1* cKO SNs at P3. Scale bar: 20μm (left panels), 1μm (right panels)
911 **(F)** Representative images of semithin (left panels) and TEM (right panels) of transverse sections
912 of WT and *Tead1* cKO SNs at P22. Scale bar: 20μm (left panels), 1μm (right panels)
913 **(G)** Representative images of semithin (left panels) and TEM (right panels) of transverse
914 sections of WT and *Tead1* cKO SNs at P50. Scale bar: 20μm (left panels), 1μm (right panels)
915 **(H)** Quantification of G-ratio for axons in WT and *Tead1* cKO SNs at P22 and at P50. n = 3
916 mice per group. ns, p > 0.05 (P22 WT versus P50 WT, P22 cKO versus P50 cKO), ****P <
917 0.0001 (P22 WT versus P22 cKO, P50 WT versus P50 cKO).
918 **(I)** Scatter plot graph displaying G-ratio in relation to axon diameter in WT and *Tead1* cKO SNs
919 at P22. n = 1063 axons from 3 mice per each genotype.
920 **(J)** Scatter plot graph displaying G-ratio in relation to axon diameter in WT and *Tead1* cKO SNs
921 at P50. n = 880 axons from 3 mice per each genotype.
922 **(K)** Quantitative comparison of mean axon diameter in WT and *Tead1* cKO SNs at P22 and at
923 P50. n = 3 mice per group. ns, p > 0.05, *p ≤ 0.05, 2-way ANOVA with Tukey's multiple
924 comparisons test.
925 **(L)** Representative TEM images of transverse sections of P50 WT and *Tead1* cKO SNs. Right
926 panels are enlarged images of the boxed area in left panels. Scale bar: 1μm
927 **(M)** Quantification of normal and abnormal C-fibers in P50 WT and *Tead1* cKO SNs. C-fibers
928 normally ensheathed by SC cytoplasm are marked as 'ensheathed', whereas those not ensheathed
929 are denoted as 'naked'. Naked C-fibers located in a myelinated bundle are denoted as 'naked
930 myelinated'. Relative percentage of each type of C-fiber is plotted. N > 500 C-fibers from 3 mice
931 per each genotype. *p ≤ 0.05, ***p ≤ 0.001, ****P < 0.0001, 2-way ANOVA Tukey's multiple
932 comparisons test.
933

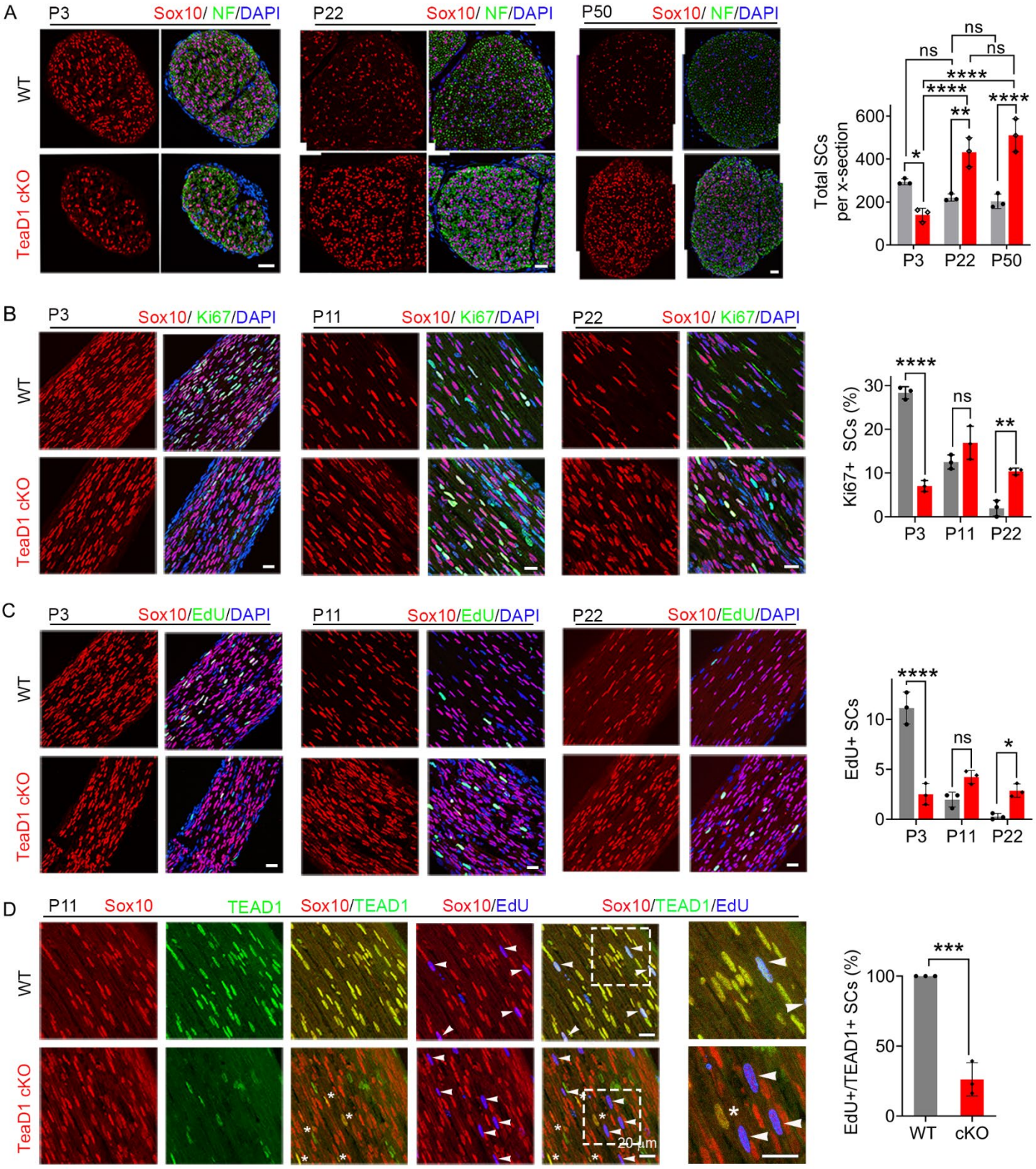
A
P3
Sox10/ NF/DAPI
P22
Sox10/ NF/DAPI
P50
Sox10/ NF/DAPI
WT
TeaD1 cKO
Total SCs per x-section
ns
ns
ns
****
****
****
**
*
600
400
200
0
P3
P22
P50
B
P3
Sox10/ Ki67/DAPI
P11
Sox10/ Ki67/DAPI
P22
Sox10/ Ki67/DAPI
WT
TeaD1 cKO
Ki67+ SCs (%)
****
ns
**
30
20
10
0
P3
P11
P22
C
P3
Sox10/EdU/DAPI
P11
Sox10/EdU/DAPI
P22
Sox10/EdU/DAPI
WT
TeaD1 cKO
EdU+ SCs
****
ns
*
10
5
0
P3
P11
P22
D
P11
Sox10
TEAD1
Sox10/TEAD1
Sox10/EdU
Sox10/TEAD1/EdU
WT
TeaD1 cKO
20 μm
EdU+/TEAD1+ SCs (%)
***
100
50
0
WT
cKO

934

935 **Figure 4. TEAD1 regulates SC proliferation both positively and negatively**

936 **(A)** Immunostaining and quantification of SCs on transverse sections of WT and *Tead1* iKO SNs
937 at P3, P22, and P52. SC nuclei and all cell nuclei are marked by Sox10 and DAPI. Axons are
938 marked by Neurofilaments (NF). n = 3 mice per genotype, ns, $p > 0.05$, *$p \leq 0.05$, **$p \leq 0.01$,
939 ****$P < 0.0001$, 2-way ANOVA with Tukey's multiple comparisons test. Scale bar: 30μm

940 **(B)** Immunostaining and quantification of Ki67+ SCs on longitudinal sections of WT and *Tead1*
941 iKO SNs at P3, P11, and P22. SC nuclei and all cell nuclei are marked by Sox10 and DAPI. n =
942 3 mice per genotype, ns, $p > 0.05$, **$p \leq 0.01$, ****$P < 0.0001$, 2-way ANOVA with Tukey's
943 multiple comparisons test. Scale bar: 30μm (P3 panels), 20μm (P11 and P22 panels)

944 **(C)** Immunostaining and quantification of EdU+ SCs on longitudinal sections of WT and *Tead1*
945 iKO SNs at P3, P11, and P22. SC nuclei and all cell nuclei are marked by Sox10 and DAPI. n =
946 3 mice per genotype, ns, $p > 0.05$, *$p \leq 0.05$, ****$P < 0.0001$, 2-way ANOVA with Tukey's
947 multiple comparisons test. Scale bar: 30μm (P3 panels), 20μm (P11 and P22 panels)

948 **(D)** Immunostaining and quantification of EdU+/TEAD1+ SCs on longitudinal sections of WT
949 and *Tead1* iKO SNs at P11. SC nuclei are marked by Sox10. Asterisks denote *Tead1* cKO SCs in
950 which TEAD1 is not deleted and which are not EdU+. Arrowheads denote EdU+ SCs which are
951 TEAD1+ in WT but TEAD1- in *Tead1* cKO. n = 3 mice per genotype, ***$P < 0.001$, Student's
952 unpaired t-test. Scale bar: 20μm

953

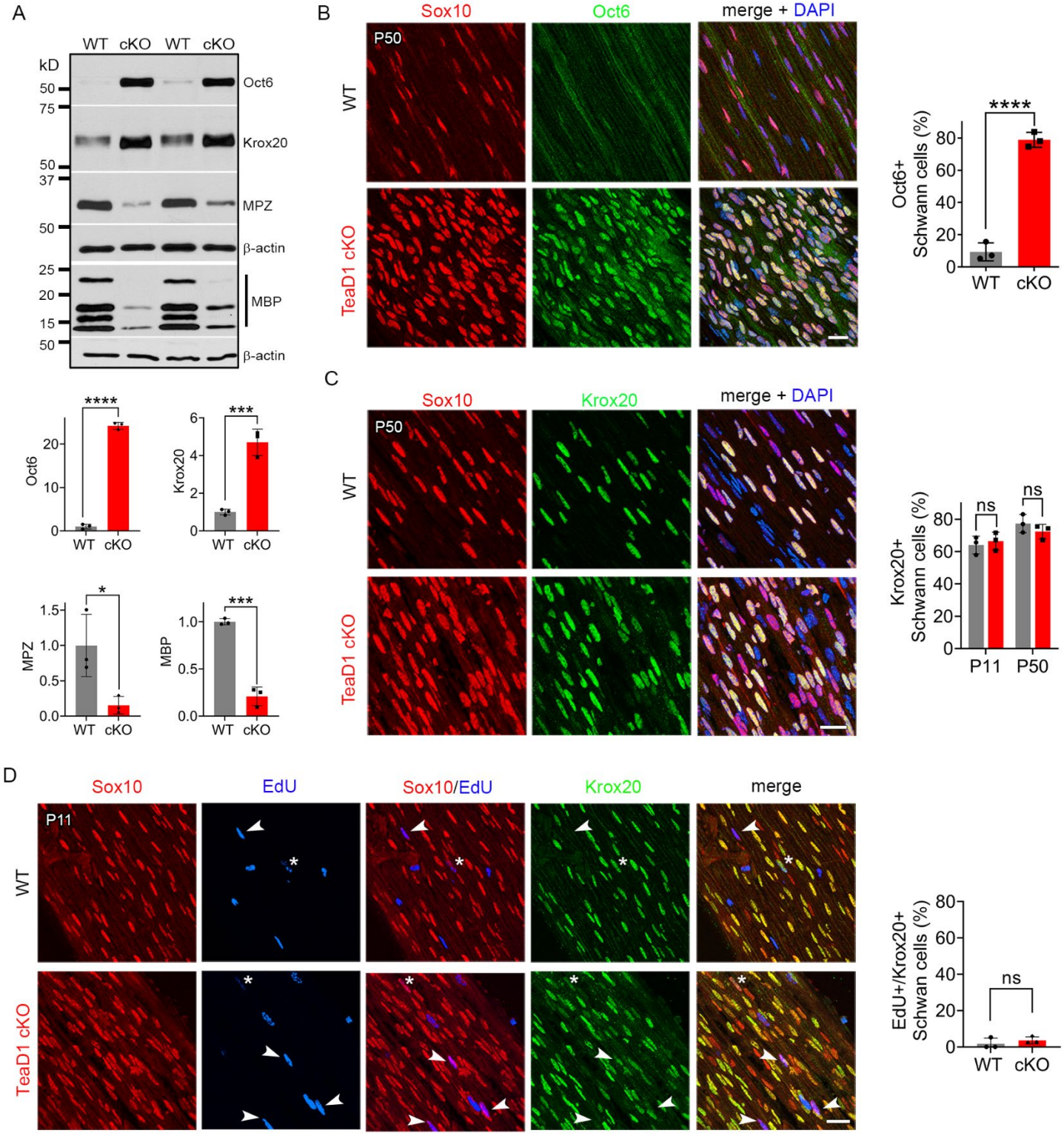
A
WT cKO WT cKO
kD
50
75
50
37
50
25
20
15
50
Oct6
Krox20
MPZ
β-actin
MBP
β-actin
Oct6
Krox20
MPZ
MBP
WT cKO
B
Sox10
Oct6
merge + DAPI
P50
WT
TeaD1 cKO
Oct6+ Schwann cells (%)
****
C
Sox10
Krox20
merge + DAPI
P50
WT
TeaD1 cKO
Krox20+ Schwann cells (%)
ns
P11 P50
D
Sox10
EdU
Sox10/EdU
Krox20
merge
P11
WT
TeaD1 cKO
EdU+/Krox20+ Schwan cells (%)
ns
WT cKO

954

955 **Figure 5. TEAD1 is required for Krox20 to upregulate myelin proteins during**
956 **development**
957 **(A)** Western blotting of P50 WT and *Tead1* cKO SN lysates with anti-Oct6, -Krox20, -MPZ, and
958 -MBP. Protein expression is normalized to that of *β-actin* as an internal control, and WT
959 expression is arbitrarily given the value 1. n = 3 mice per genotype. *$p \leq 0.05$, ***$p \leq 0.001$,
960 ***$p \leq 0.0001$, Student's unpaired t-test.
961 **(B)** Immunostaining and quantification of Oct6+ SCs on longitudinal sections of P50 WT and
962 *Tead1* cKO SNs. SC nuclei are identified by Sox10. All cell nuclei are marked by DAPI. n = 3
963 mice per genotype, ****$P < 0.0001$, Student's unpaired t-test. Scale bar: 20μm
964 **(C)** Immunostaining and quantification of Krox20+ SCs on longitudinal sections of WT and
965 *Tead1* cKO SNs at P11 and P50. SC nuclei are identified by Sox10. All cell nuclei are marked by
966 DAPI. n = 3 mice per each group, ns, $p > 0.05$, Student's unpaired t-test. Scale bar: 20μm
967 **(D)** Immunostaining and quantification of EdU+/Krox20+ SCs on longitudinal sections of WT
968 and *Tead1* cKO SNs at P11. SC nuclei are identified by Sox10. Arrowheads denote examples of
969 EdU+ SCs which are Krox20-. Asterisks denote rarely observed EdU+ SCs which are Krox20+.
970 n = 3 mice per genotype, ns, $p > 0.05$, Student's unpaired t-test. Scale bar: 20μm
971

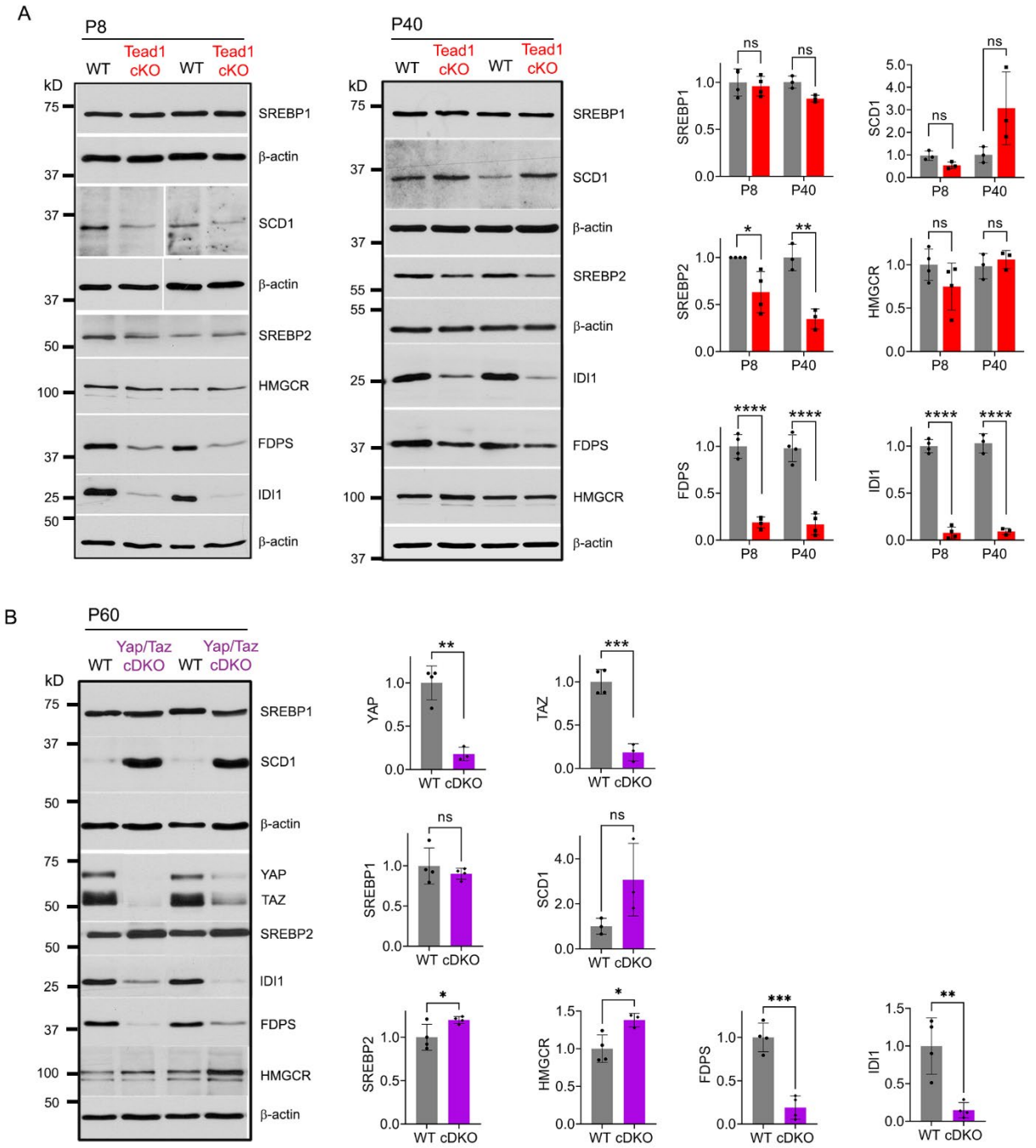

Figure 6. TEAD1 and YAP/TAZ upregulate cholesterol synthesis enzymes: FDPS and IDI1 **(A)** Western blotting of P8 and P40 WT and *Tead1* cKO SN lysates with anti-SREBP1, -SCD1, -SREBP2, -HMGCR, -FDPS, and -IDI1. Protein expression is normalized to that of *β-actin* as an internal control, and WT expression is arbitrarily given the value 1. n = 3 or 4 mice per genotype. ns, $p > 0.05$, *$p \leq 0.05$, **$p \leq 0.01$, ****$P < 0.0001$, Student's unpaired t-test. **(B)** Western blotting of P60 WT and *Yap/Taz* cDKO SN lysates with anti-YAP, -TAZ, -SREBP1, -SCD1, -

979 SREBP2, -HMGCR, -FDPS, and -IDI1. Protein expression is normalized to that of *β-actin* as an

980 internal control, and WT expression is arbitrarily given the value 1. n = 3 or 4 mice per genotype.

981 ns, $p > 0.05$, *$p \leq 0.05$, **$p \leq 0.01$, ***$P < 0.001$, Student's unpaired t-test.

982

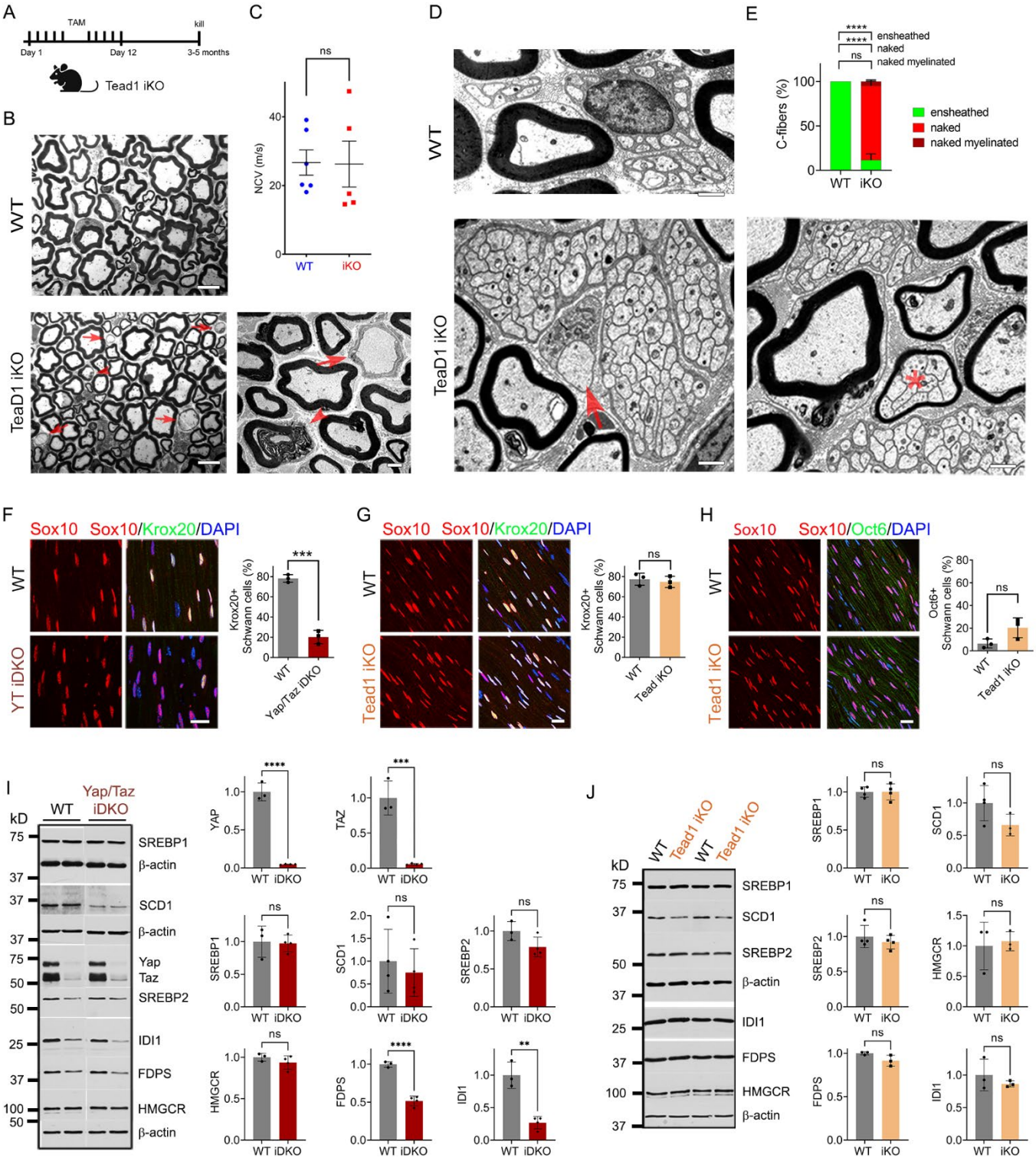

983 **Figure 7. TEAD1 is largely dispensable for myelin maintenance, but required for**
984 **preservation of Remak bundle integrity**
985 **(A)** Cartoon showing timeline of tamoxifen injection and time of sacrifice of *Tead1* iKO mice.
986 **(B)** Representative TEM images of P150 WT and *Tead1* iKO SNs showing occasional large
987 axons undergoing demyelination (arrowheads) or completely demyelinated (arrows). Scale bar:
988 6μm (left panels), 2μm (right panel)
989 **(C)** Quantification of NCV in P90-P150 WT and *Tead1* iKO mice. n = 5 or 6 mice per genotype.
990 ns, $p > 0.05$, Student's unpaired t-test.
991 **(D)** Representative TEM images of P97 WT and *Tead1* iKO SNs showing Remak bundles.
992 Asterisk denotes a bundle of thinly myelinated C-fibers. Arrow denotes demyelinated axon.
993 Scale bar: 1μm
994 **(E)** Quantification of normal and abnormal C-fibers in P150 WT and *Tead1* iKO SNs. Relative
995 percentage of each type of C-fiber is plotted. N > 500 C-fibers from 3 mice per each genotype.
996 ns, $p > 0.05$, ****$P < 0.0001$, 2-way ANOVA Tukey's multiple comparisons test.
997 **(F)** Immunostaining and quantification of Krox20+ SCs on longitudinal sections of WT and
998 *Yap/Taz* iKO SNs 2 weeks after 1st tamoxifen injection. SC nuclei are marked by Sox10. All cell
999 nuclei are marked by DAPI. n = 3 mice per genotype, ***$P < 0.001$, Student's unpaired t-test.
1000 Scale bar: 20μm
1001 **(G)** Immunostaining and quantification of Krox20+ SCs on longitudinal sections of WT and
1002 *Tead1* iKO SNs 6 weeks after 1st tamoxifen injection. SC nuclei are marked by Sox10. All cell
1003 nuclei are marked by DAPI. n = 3 mice per genotype, ns, $p > 0.05$, Student's unpaired t-test.
1004 Scale bar: 20μm
1005 **(H)** Immunostaining and quantification of Oct6+ SCs on longitudinal sections of WT and *Tead1*
1006 iKO SNs 6 weeks after 1st tamoxifen injection. SC nuclei are marked by Sox10. All cell nuclei
1007 are marked by DAPI. n = 3 mice per genotype, ns, $p > 0.05$, Student's unpaired t-test. Scale bar:
1008 20μm
1009 **(I)** Western blotting of WT and *Yap/Taz* iDKO SN lysates with anti-YAP, -TAZ, -SREBP1, -
1010 SCD1, -SREBP2, -HMGCR, -FDPS, and -IDI1. Protein expression is normalized to that of *β-*
1011 *actin* as an internal control, and WT expression is arbitrarily given the value 1. n = 3 or 4 mice
1012 per genotype. ns, $p > 0.05$, **$p \leq 0.01$, ***$P < 0.001$, ****$P < 0.0001$, Student's unpaired t-test.

(J) Western blotting of WT and *Tead1* iKO SN lysates with anti-SREBP1, -SCD1, -SREBP2, -HMGCR, -FDPS, and -IDI1. Protein expression is normalized to that of *β-actin* as an internal control, and WT expression is arbitrarily given the value 1. n = 3 or 4 mice per genotype. ns, $p > 0.05$, Student's unpaired t-test.

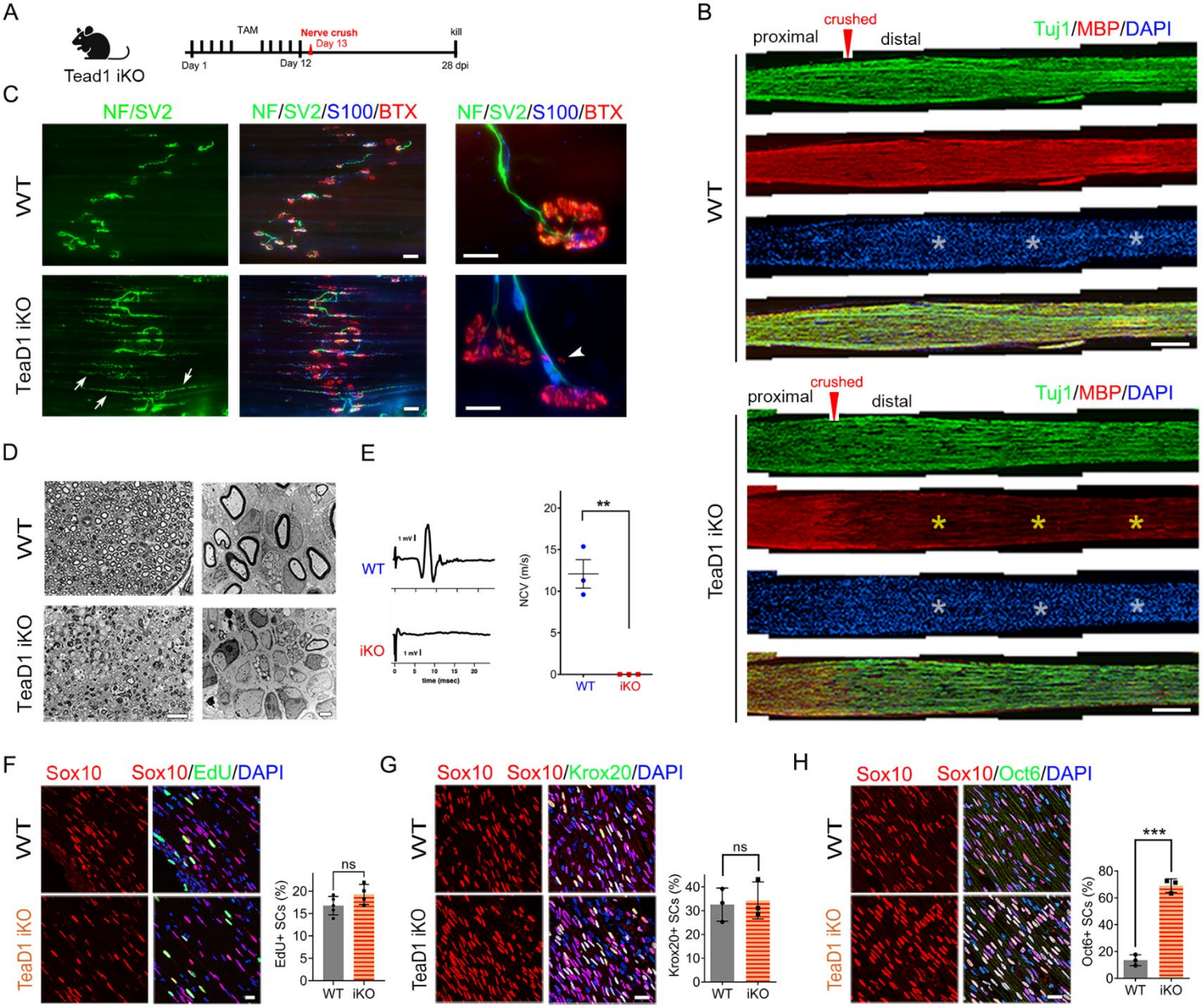

Figure 8. TEAD1 is required for functional regeneration of peripheral nerve

1020 **(A)** Cartoon showing timeline of tamoxifen injection and time of sacrifice of *Tead1* iKO mice
1021 after nerve crush.
1022 **(B)** Low magnification images of longitudinal sections of ~4mm long SN segments of WT and
1023 *Tead1* iKO mice 28 days after nerve crush. Arrowheads denote crush site. Axons and myelin are
1024 marked by Tuj1 and MBP, respectively. All cell nuclei are marked by DAPI. Yellow asterisks
1025 denote the distal nerve segment of *Tead1* iKO, which almost completely lacks myelin. White
1026 asterisks denote distal segments of both WT and *Tead1* iKO, which exhibit more cells than
1027 proximal segments due to SC proliferation after injury. Scale bar: 500μm
1028 **(C)** Representative low and high magnification NMJ images of WT and Tead1 iKO 28 days after
1029 nerve crush. Axon and axon terminals are marked by neurofilament (NF) and SV2 staining. SCs
1030 are marked by S100. Muscle acetylcholine receptors are marked by α-Bungarotoxin. Arrows
1031 denote examples of axon terminals that grew past NMJs in iKO. Arrowheads denote examples of
1032 extrasynaptic AChR clusters in iKO. Scale bar: 50μm (low magnification panels), 20μm (high
1033 magnification panels)
1034 **(D)** Representative semi-thin and TEM images of transverse sections of WT and *Tead1* iKO 28
1035 days after nerve crush. Scale bar: 20μm (left semi-thin panels), 2μm (right TEM panels)
1036 **(E)** Representative CMAP recordings and NCV measurements of WT and *Tead1* iKO at 28 days
1037 after nerve crush. n = 3 mice per genotype, $^{**}p \leq 0.01$, Student's unpaired t-test.
1038 **(F)** Immunostaining and quantification of EdU+ SCs on longitudinal sections of WT and *Tead1*
1039 iKO SNs at 28 days after nerve crush. SC nuclei are marked by Sox10. All cell nuclei are marked
1040 by DAPI. n = 4 mice per genotype, ns, $p > 0.05$, Student's unpaired t-test. Scale bar: 20μm
1041 **(G)** Immunostaining and quantification of Krox20+ SCs on longitudinal sections of WT and
1042 *Tead1* iKO SNs at 28 days after nerve crush. SC nuclei are marked by Sox10. All cell nuclei are
1043 marked by DAPI. n = 3 mice per genotype, ns, $p > 0.05$, Student's unpaired t-test. Scale bar:
1044 20μm
1045 **(H)** Immunostaining and quantification of Oct6+ SCs on longitudinal sections of WT and *Tead1*
1046 iKO SNs at 28 days after nerve crush. SC nuclei are marked by Sox10. All cell nuclei are marked
1047 by DAPI. n = 3 mice per genotype, ns, $^{***}P < 0.001$, Student's unpaired t-test. Scale bar: 20μm
1048
1049 **FUNDINGS**

This work was supported by grants from Shriners Children's (#84050 to Y-J.S.) and NIH NINDS (NS105796 to Y-J.S.).

AUTHOR CONTRIBUTIONS

Conceptualization: MG, YS

Methodology: GH, JZ

Investigation: MG, HK, SP, JA, ML, YS

Funding acquisition: YS

Supervision: ML, YS

Writing – original draft: MG

Writing – review & editing: YS

COMPETING INTERESTS

The authors declare no competing interests.

DATA AND MATERIALS AVAILABILITY

All data are available in the main text or the supplementary materials.

1 **SUPPLMENTARY MATERIALS (Grove et al.)**

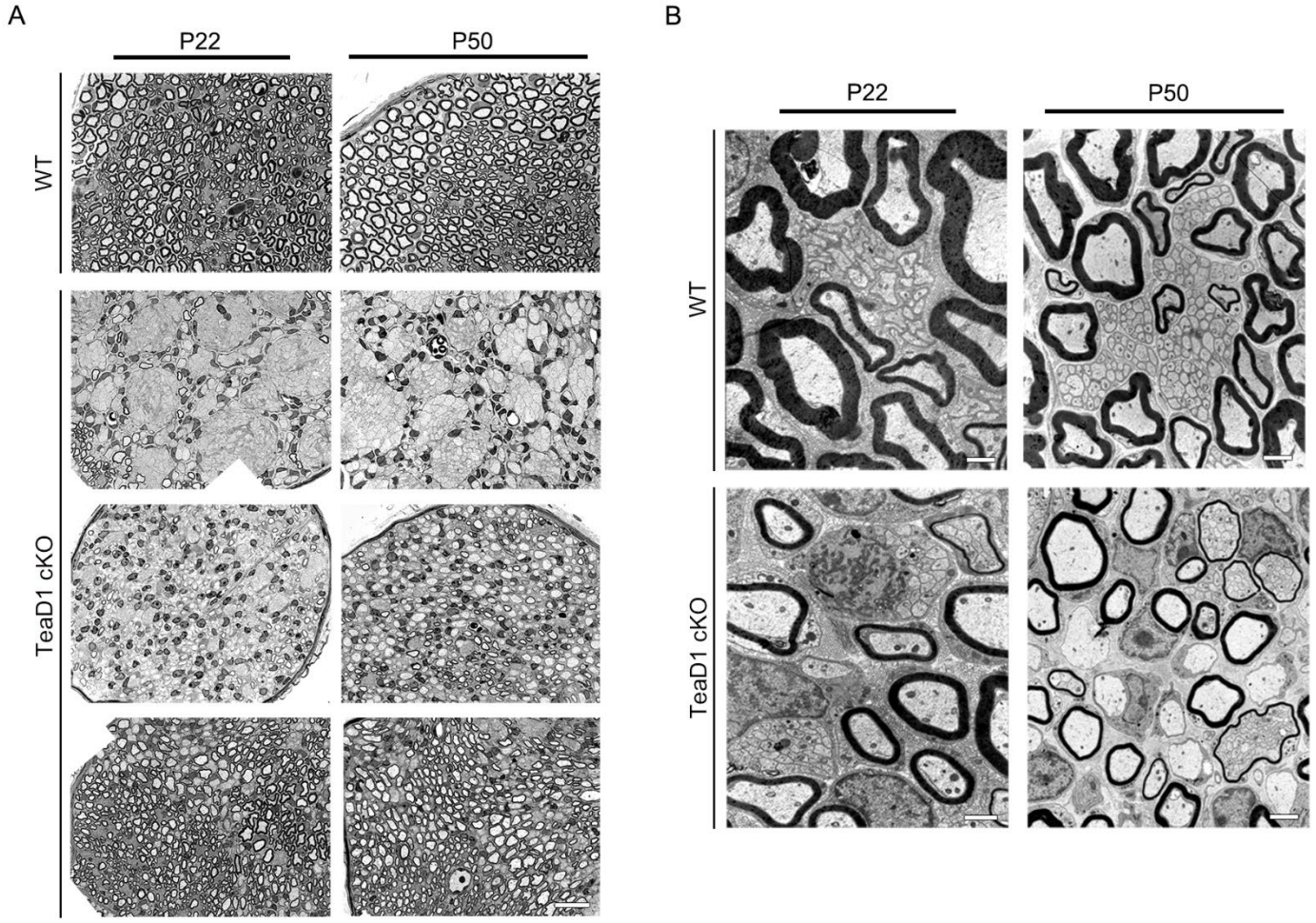

2 **Supplementary figure 1. Additional semi-thin and TEM images of WT and *Tead1* cKO**

3 **(A)** Representative images of semi-thin sections of various areas of WT and Tead1 cKO SNs at

4 P22 and P50. Scale bar: 20µm

5 **(B)** Representative TEM images of transverse sections of WT and Tead1 cKO SNs at P22 and

6 P50. Scale bar: 1µm (P22 panels), 2µm (P50 panels)

7

8 **Supplementary video 1. A movie showing a P55 WT and two littermates *Tead1* cKO mice**